

## Multicolor photometry of the galaxy cluster A98: substructures and star formation properties \*

Li Zhang<sup>1</sup>, Qi-Rong Yuan<sup>1</sup>, Xu Zhou<sup>2</sup>, Zhao-Ji Jiang<sup>2</sup>, Yan-Bin Yang<sup>2</sup>, Jun Ma<sup>2</sup>,  
Jiang-Hua Wu<sup>2</sup> and Zhen-Yu Wu<sup>2</sup>

<sup>1</sup> Department of Physics, Nanjing Normal University, Nanjing 210046, China;  
[yuanqirong@njnu.edu.cn](mailto:yuanqirong@njnu.edu.cn); [lizhang722@163.com](mailto:lizhang722@163.com)

<sup>2</sup> National Astronomical Observatories, Chinese Academy of Sciences, Beijing 100012, China

Received 2009 August 21; accepted 2009 September 24

**Abstract** An optical photometric observation with the Beijing–Arizona–Taiwan–Connecticut (BATC) multicolor system is carried out for A98 ( $z = 0.104$ ), a galaxy cluster with two large enhancements in X-ray surface brightness. Spectral energy distributions (SEDs) covering 15 intermediate bands are obtained for all sources detected down to  $V \sim 20$  mag in a field of  $58' \times 58'$ . After star–galaxy separation with color–color diagrams, a photometric redshift technique is applied to the galaxy sample for further membership determination. The color–magnitude relation is taken as a further restriction of the early-type cluster galaxies. As a result, a list of 198 faint member galaxies is achieved. Based on the newly generated sample of member galaxies, the dynamical substructures, A98N, A98S, and A98W, are investigated in detail. A separate galaxy group, A98X, is also found to the south of the main concentration of A98, which is gravitationally unbound to A98. For 74 spectroscopically confirmed member galaxies, the environmental effect on the star formation history is investigated. The bright galaxies in the core region are found to have shorter time scales of star formation, longer mean stellar ages, and higher interstellar medium metallicities, which can be interpreted in the context of the hierarchical cosmological scenario.

**Key words:** galaxies: clusters: individual (A98) – galaxies: distances and redshifts — galaxies: kinematics and dynamics — galaxies: evolution — methods: data analysis

### 1 INTRODUCTION

Following the hierarchical scenario of structure formation, massive clusters form through episodic mergers of subunits, such as groups and poor clusters, and through the continuous accretion of field galaxies along filaments (Zeldovich et al. 1982; West et al. 1991, 1995; Colberg et al. 2000). Both X-ray and optical surveys have revealed a significant level of substructure in rich galaxy clusters (Rhee et al. 1991; Forman & Jones 1982; Beers et al. 1991; Sarazin 1992; Henry & Briel 1993; Burns et al. 1994). Numerical simulation of the evolution of galaxy clusters indicates that at least 50% of apparently relaxed clusters contain significant substructures (Salvador-Sole et al. 1993). The

---

\* Supported by the National Natural Science Foundation of China.

dynamics of these “lumpy” clusters thus provide a means for exploring cluster evolution, which may shed light on the theories of large-scale structure formation (Kauffmann et al. 1999).

A98 is a good example of clusters with multiple components. It is a rich ( $R = 3$ ), quite distant ( $z = 0.1042$ ,  $D = 5$ ) cluster (Abell et al. 1989) without a large cD galaxy at its center (the Bautz–Morgan type -BM:II–III). It was first selected optically by Abell (1958), and was regarded as a single galaxy cluster before the launch of the *Einstein* Observatory (Duus & Newell 1977). The X-ray surface brightness distribution of A98 exhibits two large enhancements which are considered to be associated with the north and south components (Forman et al. 1981; Henry et al. 1981; Jones & Forman 1999). From then, A98 was extensively studied as a typical double cluster. Dressler (1978a,b) analyzed the galaxy distribution of A98, and suggested that it consists of two subclusters, namely the south (A98S) and the north (A98N) ones. The radial velocities for galaxies in A98 have been discussed by many authors (Faber & Dressler 1977; Dressler 1978b; Beers et al. 1982; Zabludoff et al. 1990). However, the number of spectroscopically confirmed member galaxies in A98 in previous studies is very limited. Based on only 24 member galaxies, Beers et al. (1982, hereafter BGH) estimated the virial masses and mass to luminosity ratios of A98N and A98S. By using the two-body model, they further calculated the probability of gravitational binding, and derived that the two subclusters would merge in another 3 billion years. Krempel-Krygier & Krygier (1995, hereafter KK95) studied the dynamics of A98 on the basis of only 29 cluster members. As a rich cluster containing wide-angle tailed (WAT) radio galaxies, A98 is included in the sample of WAT-containing clusters in Pinkney et al. (2000, hereafter PBLGH). The redshifts of some galaxies in the A98 region were obtained in that paper, but they did not investigate the dynamics of A98 in detail.

Substructures in the optical surface density and radial velocity are the typical signatures that allow the identification of merging clusters. In this paper, we collect 74 cluster galaxies with known spectroscopic redshifts from the literature, and investigate the dynamical substructures in A98. For a better understanding of the dynamics of A98, the faint member galaxies ( $18.0 < m_V < 20.0$ ) should be taken into account. This paper will present multicolor photometry of the galaxies in A98 with the Beijing–Arizona–Taiwan–Connecticut (BATC) system. Based on the spectral energy distributions (SEDs) of faint galaxies, we try to supplement a large number of new member galaxies by applying the photometric redshift technique. The enlarged data set may verify the spatial distribution and dynamical properties of A98 to an unprecedented depth. Additionally, the star formation histories of the bright member galaxies may help us to understand the evolution of A98.

This paper is organized as follows. In Section 2, we present the BATC multicolor photometric observations and data reduction. In Section 3, we analyze the galaxies with known spectroscopic redshifts in the A98 field, and distinguish a new galaxy group at  $z = 0.12$  from the main concentration of A98. Section 4 presents the SED selection of faint member galaxies of A98. In Section 5, the dynamical substructures and star formation properties are investigated on the basis of the sample of spectroscopically confirmed members and the enlarged sample of member galaxies. Finally, we summarize our work in Section 6. Throughout this paper, we assume the cosmological parameters  $H_0 = 70 \text{ km s}^{-1} \text{ Mpc}^{-1}$ ,  $\Omega_m = 0.3$  and  $\Omega_\Lambda = 0.7$ .

## 2 OBSERVATION AND DATA REDUCTION

The BATC multicolor photometric survey is designed to obtain optical SED information on faint objects without spectroscopic observation using the 60/90 cm  $f/3$  Schmidt telescope of the National Astronomical Observatories, Chinese Academy of Sciences (NAOC), located at the Xinglong site at an altitude of 900 m. Before October 2006, an old Ford CCD camera with a format of  $2048 \times 2048$  was mounted at the main focus of the telescope. The field of view was  $58' \times 58'$ , with a scale of  $1.7'' \text{ pixel}^{-1}$ . For better spatial resolution and higher sensitivity in blue bands, a new E2V 4096  $\times$  4096 CCD camera has since been installed. The field of view has become larger ( $92' \times 92'$ ) with

**Table 1** Parameters of the BATC Filters and the Observational Statistics of A98

| No. | Filter name | $\lambda_c^a$<br>(Å) | FWHM<br>(Å) | Exposure<br>(s) | Number of<br>Images | Seeing <sup>b</sup><br>(arcsec) | Objects<br>Detected | Completeness<br>magnitude |
|-----|-------------|----------------------|-------------|-----------------|---------------------|---------------------------------|---------------------|---------------------------|
| 1   | a           | 3360                 | 222         | 10800           | 9                   | 4.23                            | 5107                | 21.0                      |
| 2   | b           | 3890                 | 291         | 3600            | 3                   | 3.41                            | 6860                | 20.5                      |
| 3   | c           | 4210                 | 309         | 5400            | 6                   | 3.50                            | 6900                | 20.5                      |
| 4   | d           | 4550                 | 332         | 22366           | 19                  | 4.19                            | 5753                | 20.5                      |
| 5   | e           | 4920                 | 374         | 12000           | 10                  | 3.79                            | 6643                | 20.5                      |
| 6   | f           | 5270                 | 344         | 12000           | 10                  | 4.95                            | 7977                | 20.0                      |
| 7   | g           | 5795                 | 289         | 7200            | 6                   | 4.27                            | 8122                | 20.0                      |
| 8   | h           | 6075                 | 308         | 6000            | 5                   | 4.41                            | 8125                | 19.5                      |
| 9   | i           | 6660                 | 491         | 6000            | 9                   | 4.05                            | 8108                | 19.5                      |
| 10  | j           | 7050                 | 238         | 6000            | 5                   | 7.53                            | 7503                | 19.5                      |
| 11  | k           | 7490                 | 192         | 7200            | 6                   | 3.86                            | 8010                | 19.0                      |
| 12  | m           | 8020                 | 255         | 10800           | 9                   | 4.12                            | 8119                | 19.0                      |
| 13  | n           | 8480                 | 167         | 10800           | 9                   | 4.38                            | 7928                | 19.0                      |
| 14  | o           | 9190                 | 247         | 15000           | 13                  | 3.74                            | 8106                | 18.5                      |
| 15  | p           | 9745                 | 275         | 20400           | 17                  | 4.93                            | 7609                | 18.5                      |

<sup>a</sup> Central wavelengths of the filters; <sup>b</sup> This column lists the seeings of the combined images.

a spatial scale of  $1.35'' \text{ pixel}^{-1}$ . The pixel sizes for the old and new CCD cameras are  $15 \mu\text{m}$  and  $12 \mu\text{m}$ , respectively, and the pixel size ratio is exactly 5:4. The newly equipped CCD camera has a high quantum efficiency of 92.2% at  $4000 \text{ \AA}$ . The BATC filter system contains 15 intermediate-band filters covering the wavelength range from  $3000$  to  $10000 \text{ \AA}$ . These filters were especially designed to avoid bright night sky emission lines (Fan et al. 1996). The transmission curves can be found in Yuan et al. (2003) and Xia et al. (2002).

From 1996 to 2006, we accumulated 37 h in only 12 bands, from *d* to *p*, with the old CCD camera. In the last two years, exposures in the *a*, *b*, and *c* filters were completed with the new CCD camera. The total exposure time has reached more than 42 h (see the observational statistics in Table 1). With automatic data-processing software, PIPELINE I (Fan et al. 1996), we carried out the standard procedures of bias subtraction, flat-field correction, and position calibration. The technique of integral pixel shifting was used in the image combination, during which cosmic rays and bad pixels were removed by comparing multiple images.

For detecting and measuring the flux of sources within a given aperture in the BATC images, we use a photometry package, PIPELINE II, developed on the basis of the DAOPHOT kernel (Zhou et al. 2003a), to perform aperture photometry. An object is considered to be detected if its signal to noise ratio is larger than the threshold  $3.5\sigma$  in *i*, *j*, and *k* bands. Because the pixel size ratio between the old and new CCDs is 5:4, we adopt a radius of 4 pixels as the photometric aperture for the images in 12 bands (from *d* to *p*), and a radius of 5 pixels for the images in the other three bands (from *a* to *c*). The flux calibration in the *h* band is performed using the Oke–Gunn primary flux standard star HD 19445, HD 84937, BD+26 2606, and BD+17 4708 (Gunn & Stryker 1983). To achieve the *relative* SEDs of the sources detected by the BATC system, Zhou et al. (1999) developed a method of model calibration on the basis of the stellar SED library. No calibration images of the standard stars are needed during the flux calibration. As a result, using this model calibration method, the SEDs of about 9000 sources have been obtained for further analysis.

The magnitude within a fixed photometric aperture is somewhat different from the total magnitudes of galaxies given in some catalogs. To assess the measurement errors at specified magnitudes, we separate stars into different bins of magnitude with an interval of 0.5 mag, and we find that the magnitude error in each filter is larger at fainter depths. A typical error is less than 0.02 mag for stars brighter than 16.5 mag, and about 0.05 mag for stars with  $V \sim 18.5$  mag.

### 3 DISCOVERY OF A NEW GALAXY GROUP ‘A98X’

#### 3.1 Distribution of Spectroscopic Redshifts

To study the dynamics of the galaxy cluster A98, 122 galaxies with known spectroscopic redshifts ( $z_{\text{sp}}$ ) in the  $58' \times 58'$  field centered at A98 are extracted from the NASA/IPAC Extragalactic Database (NED). Most of the spectroscopic data were contributed by Struble & Rood (1999) who present a compilation of the redshifts for 1572 rich clusters in Abell et al. (1989). Figure 1(a) shows the distribution of spectroscopic redshifts of these bright galaxies. The highest peak, centered at  $z_{\text{sp}} \sim 0.104$ , is isolated and less contaminated. Hence, it is unambiguous to regard the 74 galaxies with  $0.095 < z_{\text{sp}} < 0.115$  as spectroscopically confirmed member galaxies in A98, and we refer to these member galaxies as ‘sample I.’ Table 2 lists information on the position and spectroscopic redshift of these 74 galaxies.

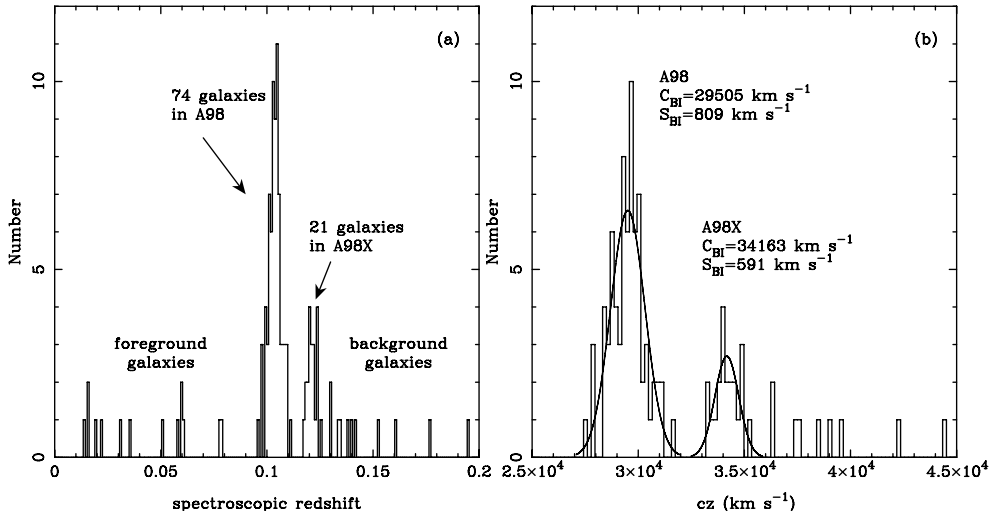


**Fig. 1** *Left*: Distribution of spectroscopic redshifts for 122 known galaxies in the A98 region. The bin size is 0.00125. *Right*: Distribution of radial velocities for the galaxies in A98 and A98X, with a Gaussian fitting superimposed on each component.

To quantify the velocity distribution of member galaxies, we firstly convert the redshifts into true cosmological velocities by  $v = c[(1 + z_{\text{sp}})^2 - 1]/[(1 + z_{\text{sp}})^2 + 1]$ , where  $c$  is the light speed. Then, we use the ROSTAT software (Beers, Flynn & Gebhardt 1990) to calculate two resistant and robust estimators analogous to the velocity mean and standard deviation, namely, the biweight location ( $C_{\text{BI}}$ ) and scale ( $S_{\text{BI}}$ ). For these 74 member galaxies, we achieve  $C_{\text{BI}} = 29505 \pm 94 \text{ km s}^{-1}$  and  $S_{\text{BI}} = 809 \pm 77 \text{ km s}^{-1}$ . Figure 1(b) shows the distribution of the line-of-sight velocities for these 74 galaxies. Taking a cosmological correction factor of  $(1 + z)^{-1}$  into account, the velocity dispersion of A98 should be  $732 \pm 70 \text{ km s}^{-1}$ .

Our sample of member galaxies is much larger than the ones in BGH and KK95. Based on only 29 member galaxies, KK95 derived a mean velocity of  $29757 \text{ km s}^{-1}$  and a velocity dispersion of  $859 \text{ km s}^{-1}$ . Using 69 member galaxies in A98, PBLGH derived a mean velocity of  $31085 \pm 96 \text{ km s}^{-1}$  and a velocity dispersion of  $797 \pm 73 \text{ km s}^{-1}$ . Their values are larger than our estimates due to the contamination of the galaxy group at  $z = 0.120$ , which will be discussed in the next subsection.

**Table 2** Catalog of Spectroscopically Confirmed Member Galaxies in A98

| No. | R.A.      | Decl     | $z_{\text{sp}}$ | Ref. | No. | R.A.      | Decl     | $z_{\text{sp}}$ | Ref. |
|-----|-----------|----------|-----------------|------|-----|-----------|----------|-----------------|------|
| 1   | 0 45 33.0 | 20 15 09 | 0.1003          | (1)  | 38  | 0 46 24.7 | 20 37 19 | 0.1028          | (2)  |
| 2   | 0 45 40.2 | 20 15 58 | 0.0999          | (1)  | 39  | 0 46 25.8 | 20 29 06 | 0.1094          | (2)  |
| 3   | 0 45 41.3 | 20 31 01 | 0.1030          | (1)  | 40  | 0 46 25.9 | 20 27 33 | 0.1041          | (3)  |
| 4   | 0 45 41.3 | 20 28 02 | 0.0961          | (1)  | 41  | 0 46 26.8 | 20 36 52 | 0.0995          | (1)  |
| 5   | 0 45 45.5 | 20 26 17 | 0.1045          | (2)  | 42  | 0 46 28.5 | 20 23 49 | 0.1013          | (4)  |
| 6   | 0 45 46.9 | 20 26 57 | 0.1043          | (3)  | 43  | 0 46 29.3 | 20 28 05 | 0.1032          | (3)  |
| 7   | 0 45 48.1 | 20 27 36 | 0.1034          | (2)  | 44  | 0 46 29.5 | 20 33 19 | 0.1045          | (3)  |
| 8   | 0 45 48.6 | 20 26 06 | 0.1039          | (1)  | 45  | 0 46 29.8 | 20 38 58 | 0.1088          | (3)  |
| 9   | 0 45 50.1 | 20 29 10 | 0.1012          | (1)  | 46  | 0 46 29.9 | 20 34 28 | 0.0978          | (1)  |
| 10  | 0 45 50.4 | 20 27 49 | 0.1037          | (4)  | 47  | 0 46 30.1 | 20 36 49 | 0.0980          | (3)  |
| 11  | 0 45 50.5 | 20 29 07 | 0.1033          | (1)  | 48  | 0 46 31.1 | 20 31 44 | 0.1034          | (1)  |
| 12  | 0 45 57.4 | 20 36 56 | 0.1013          | (1)  | 49  | 0 46 31.8 | 20 28 11 | 0.1082          | (2)  |
| 13  | 0 45 59.3 | 20 23 50 | 0.1058          | (1)  | 50  | 0 46 32.0 | 20 28 27 | 0.1048          | (1)  |
| 14  | 0 46 02.1 | 20 30 51 | 0.0996          | (1)  | 51  | 0 46 32.1 | 20 43 06 | 0.1046          | (1)  |
| 15  | 0 46 02.2 | 20 30 30 | 0.1060          | (1)  | 52  | 0 46 32.5 | 20 28 24 | 0.1060          | (1)  |
| 16  | 0 46 04.0 | 20 34 51 | 0.1005          | (3)  | 53  | 0 46 33.9 | 20 23 55 | 0.1091          | (1)  |
| 17  | 0 46 04.5 | 20 36 45 | 0.1044          | (4)  | 54  | 0 46 35.2 | 20 30 11 | 0.1041          | (1)  |
| 18  | 0 46 04.7 | 20 28 28 | 0.1054          | (1)  | 55  | 0 46 35.2 | 20 20 32 | 0.1024          | (1)  |
| 19  | 0 46 07.4 | 20 28 49 | 0.1059          | (1)  | 56  | 0 46 35.6 | 20 29 43 | 0.1067          | (3)  |
| 20  | 0 46 07.8 | 20 38 47 | 0.1060          | (1)  | 57  | 0 46 36.2 | 20 28 27 | 0.1073          | (3)  |
| 21  | 0 46 08.0 | 20 40 45 | 0.1019          | (2)  | 58  | 0 46 37.0 | 20 26 07 | 0.1023          | (4)  |
| 22  | 0 46 08.4 | 20 28 51 | 0.1013          | (3)  | 59  | 0 46 38.1 | 20 28 41 | 0.1033          | (1)  |
| 23  | 0 46 14.7 | 20 23 43 | 0.1034          | (1)  | 60  | 0 46 38.5 | 20 22 54 | 0.1037          | (4)  |
| 24  | 0 46 15.5 | 20 33 20 | 0.1001          | (1)  | 61  | 0 46 43.2 | 20 36 05 | 0.1045          | (3)  |
| 25  | 0 46 15.8 | 20 32 06 | 0.1024          | (1)  | 62  | 0 46 48.0 | 20 30 55 | 0.1036          | (1)  |
| 26  | 0 46 15.8 | 20 38 09 | 0.1072          | (3)  | 63  | 0 46 49.2 | 20 27 24 | 0.0978          | (1)  |
| 27  | 0 46 15.8 | 20 39 08 | 0.1075          | (2)  | 64  | 0 46 50.0 | 20 27 08 | 0.1055          | (1)  |
| 28  | 0 46 16.0 | 20 30 19 | 0.1017          | (2)  | 65  | 0 46 51.5 | 20 30 23 | 0.1019          | (1)  |
| 29  | 0 46 18.5 | 20 33 14 | 0.1051          | (1)  | 66  | 0 46 51.8 | 20 30 43 | 0.1062          | (1)  |
| 30  | 0 46 19.2 | 20 28 12 | 0.1016          | (1)  | 67  | 0 46 52.6 | 20 25 23 | 0.1086          | (1)  |
| 31  | 0 46 19.3 | 20 29 42 | 0.1098          | (2)  | 68  | 0 46 52.8 | 20 41 00 | 0.1051          | (3)  |
| 32  | 0 46 20.3 | 20 28 59 | 0.1014          | (1)  | 69  | 0 46 56.5 | 20 27 05 | 0.1009          | (1)  |
| 33  | 0 46 20.6 | 20 29 08 | 0.1032          | (1)  | 70  | 0 46 56.9 | 20 40 25 | 0.1031          | (2)  |
| 34  | 0 46 21.6 | 20 42 31 | 0.1046          | (1)  | 71  | 0 47 01.7 | 20 23 18 | 0.1049          | (1)  |
| 35  | 0 46 21.9 | 20 29 05 | 0.1116          | (3)  | 72  | 0 47 09.4 | 20 29 17 | 0.1051          | (1)  |
| 36  | 0 46 23.8 | 20 30 01 | 0.0998          | (2)  | 73  | 0 47 13.0 | 20 29 41 | 0.1069          | (1)  |
| 37  | 0 46 24.6 | 20 30 06 | 0.1043          | (3)  | 74  | 0 47 18.0 | 20 22 01 | 0.1049          | (1)  |

References: (1) Pinkney et al. (2000); (2) Zabludoff et al. (1990); (3) Beers et al. (1982); (4) Bettoni et al. (2006).

### 3.2 The South Clump ‘A98X’ at $z = 0.120$

It is interesting to find in Figure 1 that there are 21 galaxies with redshifts between 0.115 and 0.128. For this velocity concentration, we obtain a biweight location of  $C_{\text{BI}} = 34163 \pm 133 \text{ km s}^{-1}$  and a biweight scale of  $S_{\text{BI}} = 591 \pm 76 \text{ km s}^{-1}$ . Considering the cosmological correction, the velocity dispersion of this peak is  $528 \pm 68 \text{ km s}^{-1}$ . The separation between these two velocity peaks is about  $4658 \pm 163 \text{ km s}^{-1}$ .

The left panel of Figure 2 shows the spatial distribution for 74 member galaxies (denoted by asterisks) and 21 galaxies with redshifts between 0.115 and 0.128 (denoted by open triangles), with respect to the NED-given central position of A98 ( $00^{\text{h}}46^{\text{m}}26.6^{\text{s}}$ ,  $+20^{\circ}29'23''$ ; J2000.0). We superimpose a contour map of surface density that has been smoothed by a Gaussian window of  $\sigma = 1.6'$ . The contour map shows that these 21 galaxies with  $z_{\text{sp}} \sim 0.120$  belong to a separate clump, about  $15'$  south to the main concentration. As the separation between the two peaks is very remarkable, we refer to the south clump as ‘A98X’.

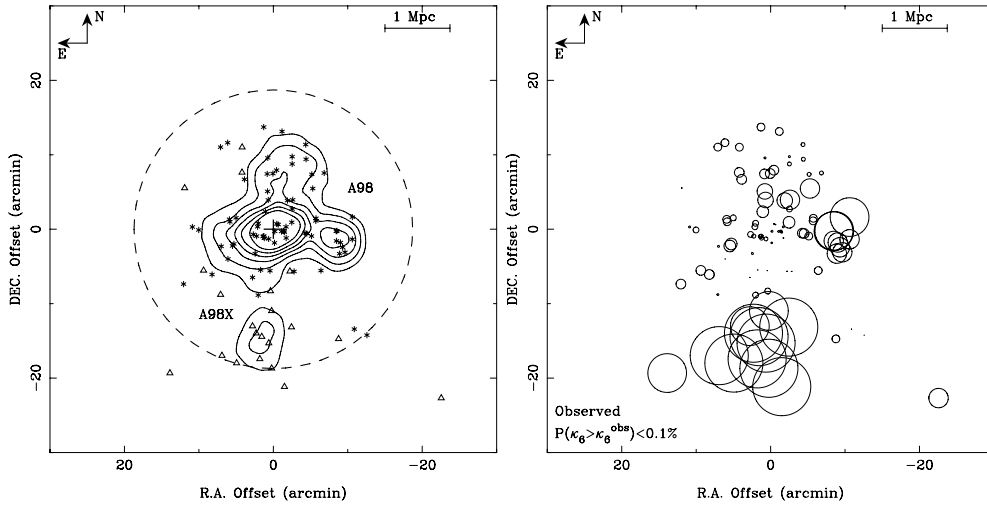


**Fig. 2** *Left*: Spatial distribution for 95 galaxies in A98 (denoted by *asterisks*) and A98X (denoted by *triangles*), superimposed on a contour map of surface density where a smoothing Gaussian window with  $\sigma = 1.6'$  is used. The contour levels are 0.09, 0.15, 0.21, 0.27, 0.33, and 0.39  $\text{arcmin}^{-2}$ , respectively. The dashed circle means a typical region of rich clusters with an Abell radius of  $1.5 h^{-1} \text{Mpc}$ ; *Right*: Bubble plot for the 95 galaxies in the A98 and A98X components.

To show the prominence of the clump A98X in both the velocity space and the projected map, we make use of the  $\kappa$ -test (Colless & Dunn 1996) for the A98/A98X system as a whole. The statistic  $\kappa_n$  is defined to quantify the local deviation on the scale of groups of  $n$  nearest neighbors. A larger  $\kappa_n$  indicates a greater probability that the local velocity distribution differs from the overall velocity distribution. The probability  $P(\kappa_n > \kappa_n^{\text{obs}})$  can be calculated by Monte Carlo simulations with random shuffling velocities. When the scale of the nearest neighbors  $n$  varies from 3 to 10, the probability  $P(\kappa_n > \kappa_n^{\text{obs}})$  is nearly zero, which means the substructure appears very obvious at different scales. The bubble plot at  $n = 6$  is given in the right panel of Figure 2. Since the bubble size is proportional to  $-\log[P_{\text{KS}}(D > D_{\text{obs}})]$ , the clustering of larger bubbles at  $(1.55', -14.43')$  can trace the significant substructure, which corresponds to the galaxy group ‘A98X’ centered at  $(0^{\text{h}}46^{\text{m}}33.2^{\text{s}}, 20^{\circ}14'57''; \text{J2000.0})$ .

We failed to find any clusters and/or groups of galaxies from the literature and existing catalogs of galaxy clusters around the position of the clump A98X. This concentration has not been mentioned in any previous investigations. An interesting question is whether the clump A98X is just a subcluster of A98 or is a newly-detected cluster/group of galaxies. To answer this question, it is necessary to verify whether A98X is gravitationally bound to the A98 cluster or not.

### 3.3 The Application of the Gravitational Binding Criterion

The masses of the main concentration of A98 and the clump A98X can be estimated by applying the virial theorem. Assuming that each cluster is bound and the galaxy orbits are random, the virial mass ( $M_{\text{vt}}$ ) can be derived from the following standard formula (Geller & Peebles 1973; Oegerle & Hill 1994):

$$M_{\text{vt}} = \frac{3\pi}{G} \sigma_r^2 D N_p \left( \sum_{i>j}^N \frac{1}{\theta_{ij}} \right)^{-1}, \quad (1)$$

where  $\sigma_r$  is the line-of-sight velocity dispersion,  $D$  is the cosmological distance of the cluster,  $N_p = N(N - 1)/2$  is the number of galaxy pairs, and  $\theta_{ij}$  is the angular separation between the galaxies  $i$  and  $j$ . The virial masses of  $9.12 \times 10^{14} M_\odot$  and  $7.98 \times 10^{14} M_\odot$  are derived for A98 and A98X, respectively. Then we specify the limits of the bound solutions by using the Newtonian criterion of gravitational binding (Beers et al. 1982):

$$V_r^2 R_p \leq 2GM \sin^2 \alpha \cos \alpha, \quad (2)$$

where  $V_r$  is the relative velocity along the line of sight,  $R_p$  is the projected separation,  $M$  is the total mass of the two clusters, and  $\alpha$  is the angle between the plane of the sky and the line connecting the two clusters. The projected separation of A98 and A98X is  $R_p = 1.78$  Mpc, and the actual observed  $V_r \sim 4200 \pm 163 \text{ km s}^{-1}$  in the rest frame of A98. The resulting constraints on  $V_r$  for bound orbits are shown in Figure 3, as a function of the projection angle,  $\alpha$ . The solid curve in this plot separates the bound and unbound regions. As the figure shows, the maximum  $V_r$  value for the bound solution is  $\sim 1800 \text{ km s}^{-1}$ , which is obviously much lower than the observed  $V_r \sim 4200 \pm 163 \text{ km s}^{-1}$ . There is no doubt that the clump A98X containing 21 galaxies is gravitationally unbound to the cluster A98. Our conclusion is that A98X is a separate group of galaxies. In our following dynamical analysis of A98, this galaxy group will be excluded.

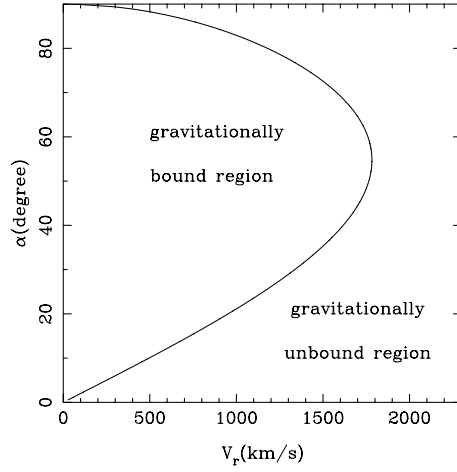


**Fig. 3** Projection angle  $\alpha$  as a function of radial velocity  $V_r$  given by the total mass  $1.71 \times 10^{15} M_\odot$ . The solid curve separates the bound and unbound regions.

It should be noted that the main concentration of A98 is not a well virialized system which contains more than two subclumps (see Sect. 5). It might be arbitrary to derive the mass of the main concentration via the virial theorem. However, we believe that the probable bias in our mass estimate is not significant enough to influence the above conclusion.

## 4 SED SELECTION OF FAINT CLUSTER GALAXIES

### 4.1 Star–Galaxy Separation

For the galaxies with known spectroscopic redshifts given by the NED, we cross-identified with the BATC-detected sources. All the sources in the BATC catalog within the searching circle (defined

by a radius of  $5''$ ) centered on the NED-given galaxies were extracted. The identification is rather unambiguous. For the case of several counterparts within the searching area, we pick up the brighter BATC source as the right counterpart. As a result, 118 bright galaxies with known  $z_{\text{sp}}$  values are identified. The 15-band SEDs of these galaxies will be used to check the reliability of our photometric redshift technique.

To select the probable faint member galaxies from the remaining BATC sources, we firstly perform the star/galaxy separation. As shown in Yuan et al. (2001), the color-color diagram is a powerful tool for classification. Since the spectra of redshifted galaxies differ significantly from those of stars, different regions in the color-color diagram are occupied by different classes of objects. Figure 4 shows two color-color diagrams used for our star–galaxy separation. The diagrams include the following categories of sources: (1) all types of stars in our SED template library (denoted by filled triangles), (2) morphologically varied galaxies with template SEDs (denoted by open circles), (3) spectroscopically confirmed member galaxies of A98 (denoted by crosses), and (4) all the remaining sources detected by BATC photometry (denoted by dots). The filters  $a(3360 \text{ \AA})$ ,  $b(3890 \text{ \AA})$ ,  $h(6075 \text{ \AA})$ , and  $p(9745 \text{ \AA})$  are used in the diagrams. It can be seen in Figure 4 that the stars in the SED template library lie in a well-defined zone stretching from top left to bottom right, while the confirmed galaxies are distributed just above the zone. Taking the dashed lines in Figure 4 as the boundaries of star–galaxy separation, we pick out the galaxies simultaneously detected in at least 11 BATC bands. As a result, we obtained 1490 faint galaxies that are located within the boundaries in both panels, to which we shall apply the photometric redshift technique.

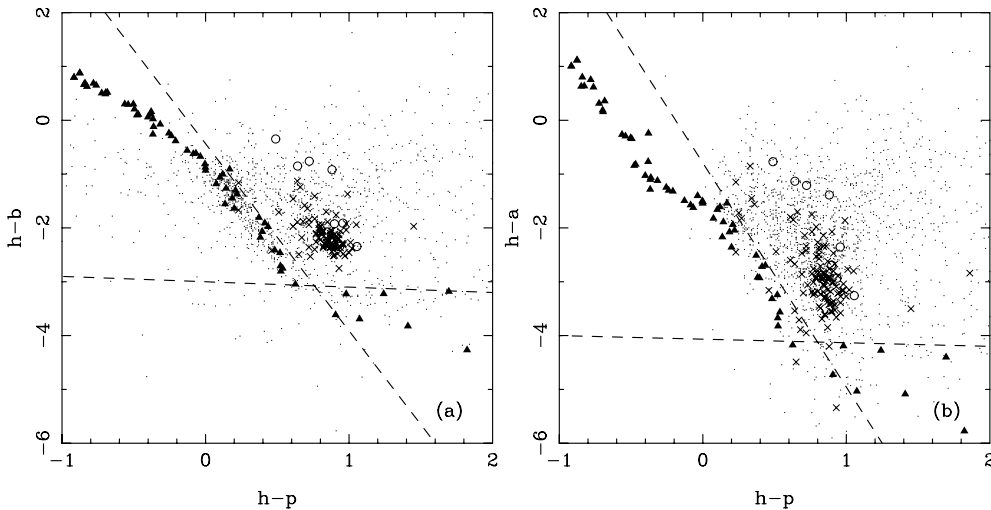


**Fig. 4** Color-color diagrams used for star–galaxy separation (*filled triangles* are for all types of stars in the SED template library, *open circles* are for various galaxies with template SEDs, *crosses* are for confirmed galaxies, *small dots* are for detected sources). The dashed lines are taken as boundaries of separation.

## 4.2 Photometric Redshifts and Cluster Membership

The technique of photometric redshift can be used to estimate the redshifts of galaxies by using SED information covering a wide range of wavelengths instead of spectroscopy. This technique is extensively applied to multicolor photometric surveys to detect faint and distant galaxies (Pelló et

al. 1999a, b; Bolzonella et al. 2000; Rowan-Robinson et al. 2008; Ilbert et al. 2009) and to select the cluster galaxies (Brunner & Lubin 2000; Finoguenov et al. 2007). For a given object, based on the standard SED-fitting code called HYPERZ (Bolzonella et al. 2000), the photometric redshift,  $z_{\text{ph}}$ , corresponds to the best fit (in the  $\chi^2$ -sense) between its photometric SED and the template SED generated by convolving the galaxy's spectra in the template library with the transmission curves of BATC filters. Previous work has evaluated the accuracy of photometric redshifts with the BATC multi-band data (Yuan et al. 2001, 2003; Zhou et al. 2003b; Yang et al. 2004). In our SED fitting, only normal galaxies are taken into account in the reference templates. Dust extinction with a reddening law of the Milky Way (Allen 1976) is adopted, and  $A_V$  is allowed to be flexible in a range from 0.0 to 0.2, in steps of 0.02. The photometric redshift of a galaxy with the BATC SED is searched from 0.0 to 0.5, in steps of 0.005.

For the 118 galaxies with known spectroscopic redshifts, a comparison between the photometric redshifts  $z_{\text{ph}}$  and the spectroscopic redshifts  $z_{\text{sp}}$  is shown in Figure 5. It is obvious that our  $z_{\text{ph}}$  estimate is basically consistent with the spectroscopic redshift. For the 74 member galaxies in sample I, the biweight location ( $C_{\text{BI}}$ ) and scale ( $S_{\text{BI}}$ ) of the  $z_{\text{ph}}$  estimate are 0.097 and 0.008, respectively. There exists a slight systematic offset in the  $z_{\text{ph}}$  distribution, with regard to the  $z_{\text{sp}}$  distribution. Taking the selection criterion of  $2\sigma$  clipping, 65 member galaxies (about 90 percent) are found to have their photometric redshifts in a range from 0.081 ( $= 0.097 - 2 \times 0.008$ ) to 0.113 ( $= 0.097 + 2 \times 0.008$ ). This  $z_{\text{ph}}$  region can be applied as a selection criterion in the subsequent membership determination for faint galaxies only detected by BATC multicolor photometry.

Figure 6 shows the histogram of photometric redshifts for faint galaxies with  $z_{\text{ph}} < 0.2$  in the field of view. The galaxies with  $0.081 < z_{\text{ph}} < 0.113$  within one Abell radius ( $1.5 h^{-1}$  Mpc), corresponding to 18.71 arcmin at  $z = 0.104$ , are selected as member candidates of A98. As a result, there are 198 faint member candidates, among which 137 galaxies are regarded as early-type galaxies and 61 galaxies are regarded as late-type galaxies by the SED-fitting procedure.

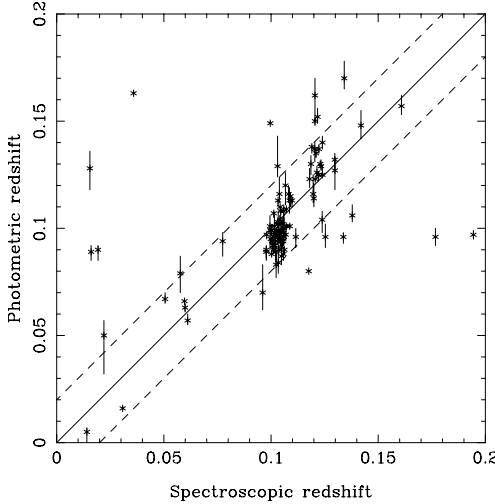


**Fig. 5** Comparison between photometric redshift  $z_{\text{ph}}$  and spectroscopic redshift  $z_{\text{sp}}$  for 118 galaxies in the field of view. The solid line corresponds to  $z_{\text{ph}} = z_{\text{sp}}$ , and the dashed lines indicate an average deviation of 0.023.

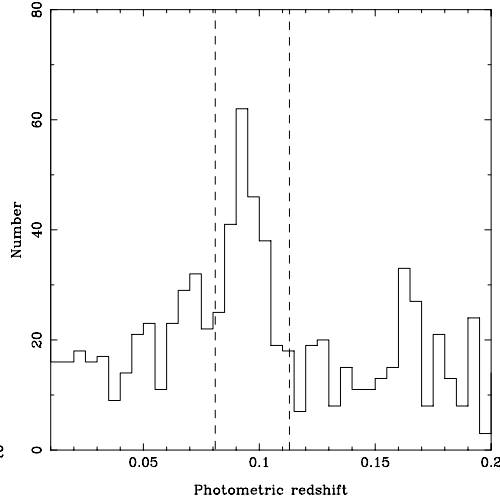


**Fig. 6** Distribution of photometric redshifts for the galaxies ( $z < 0.2$ ). The dashed lines are plotted as the photometric redshift range of cluster member candidates.

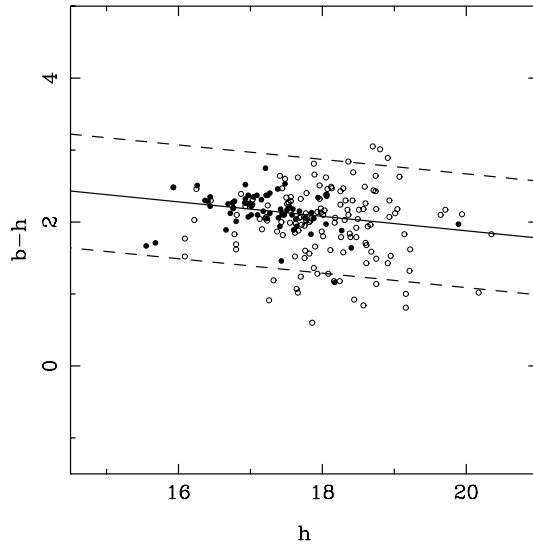


**Fig. 7** Color-magnitude correlation for 203 early-type galaxies in A98. Filled circles denote 66 early-type member galaxies which have been spectroscopically confirmed, and open circles denote 137 newly-selected member galaxies. The solid line shows the linear fit for 66 bright galaxies, and the dashed lines correspond to  $1\sigma$  deviation.

It is well known that there exists a correlation between the color and absolute magnitude for early-type galaxies (C-M relation, see Bower et al. 1992), in the sense that bright galaxies are redder, which can be used to verify the membership selection of the early-type galaxies. To select the early-type galaxies, we take the morphological types of the best-fit SED templates. Figure 7 presents a correlation between the color index  $b - h$  and magnitude in the  $h$  bandpass for 203 early-type member galaxies, including 66 early-type galaxies with known  $z_{\text{sp}}$  and 137 newly-selected early-type galaxies. The solid line denotes the linear fitting of the 66 spectroscopically confirmed member galaxies:  $b - h = -0.10(\pm 0.04)h + 3.89(\pm 0.79)$ , and the dashed lines represent  $1\sigma$  deviation. As shown in Figure 7, the majority of the early-type candidates agree with the C-M relation derived by 66 bright early-type galaxies. There are no faint early-type candidates with color  $b - h$  beyond the  $2\sigma$  deviation of the intercept. By combining the 198 newly-selected members and 74 spectroscopically confirmed member galaxies in sample I, we obtain an enlarged sample of 272 member galaxies, which is referred to as sample II.

Table 3 presents the catalog of SED information for the 198 newly selected members, as well as the celestial coordinates, photometric redshifts, and morphological classes of the best-fit template. The classification indices,  $T$ , ranging from 1 to 7 are defined to denote E, S0, Sa, Sb, Sc, Sd, and Im galaxies, respectively.

## 5 THE PROPERTIES OF THE CLUSTER A98

### 5.1 Projected Distribution of Cluster Galaxies

Figure 8 shows the projected position of the galaxies in samples I and II, superimposed with contour maps of surface density where a smoothing Gaussian window of  $\sigma = 1.6'$  is used. 74 member galaxies with known spectroscopic redshifts are denoted by filled circles and 198 photometrically selected galaxies are denoted by open circles. Two X-ray peaks given in Forman et al. (1981) are

**Table 3** Catalog of 198 Newly-selected Candidates of Member Galaxies in A98

| No. | R.A.       | Decl.       | $z_{\text{ph}}$ | $T$ | $a$   | $b$   | $c$   | $d$   | $e$   | $f$   | $g$   | $h$   | $i$   | $j$   | $k$   | $m$   | $n$   | $o$   | $p$   |
|-----|------------|-------------|-----------------|-----|-------|-------|-------|-------|-------|-------|-------|-------|-------|-------|-------|-------|-------|-------|-------|
| 1   | 0 45 07.54 | 20 30 39.10 | 0.102           | 2   | 20.94 | 20.72 | 20.26 | 19.67 | 19.26 | 18.93 | 18.69 | 18.42 | 18.20 | 18.22 | 18.01 | 17.85 | 17.71 | 17.52 | 17.43 |
| 2   | 0 45 08.17 | 20 28 21.70 | 0.099           | 5   | 19.52 | 19.01 | 18.86 | 18.32 | 18.17 | 18.04 | 17.95 | 17.82 | 17.65 | 17.66 | 17.61 | 17.48 | 17.35 | 17.26 | 17.03 |
| 3   | 0 45 11.31 | 20 27 23.60 | 0.094           | 3   | 20.09 | 20.42 | 20.03 | 18.91 | 18.87 | 18.68 | 18.45 | 18.30 | 18.14 | 18.12 | 17.87 | 17.89 | 17.67 | 17.66 | 17.76 |
| 4   | 0 45 22.06 | 20 29 56.40 | 0.087           | 1   | 19.93 | 19.34 | 19.20 | 18.70 | 18.40 | 18.34 | 18.19 | 18.16 | 18.01 | 17.72 | 17.82 | 17.81 | 17.77 | 17.62 | 17.52 |
| 5   | 0 45 24.39 | 20 39 56.80 | 0.082           | 3   | 20.21 | 19.71 | 19.66 | 19.28 | 19.05 | 19.03 | 18.83 | 18.78 | 18.66 | 18.57 | 18.55 | 18.54 | 18.48 | 18.93 | 18.60 |
| 6   | 0 45 24.63 | 20 26 22.90 | 0.099           | 2   | 20.15 | 19.47 | 19.38 | 18.46 | 17.92 | 17.65 | 17.41 | 17.24 | 17.01 | 16.98 | 16.83 | 16.73 | 16.60 | 16.42 | 16.30 |
| 7   | 0 45 24.77 | 20 41 06.10 | 0.092           | 2   | 20.51 | 19.27 | 19.22 | 18.55 | 18.21 | 17.92 | 17.65 | 17.45 | 17.19 | 17.15 | 16.96 | 16.85 | 16.71 | 16.58 | 16.51 |
| 8   | 0 45 25.61 | 20 30 51.10 | 0.101           | 1   | 20.23 | 18.91 | 18.94 | 17.94 | 17.46 | 17.22 | 17.02 | 16.81 | 16.61 | 16.32 | 16.45 | 16.34 | 16.17 | 16.07 | 15.99 |
| 9   | 0 45 31.61 | 20 22 56.20 | 0.089           | 1   | 19.37 | 18.71 | 18.50 | 18.08 | 18.00 | 17.86 | 17.71 | 17.64 | 17.62 | 17.58 | 17.64 | 17.56 | 17.51 | 17.50 | 17.39 |
| 10  | 0 45 33.45 | 20 42 21.90 | 0.092           | 1   | 20.87 | 19.76 | 19.31 | 18.61 | 18.18 | 17.90 | 17.71 | 17.51 | 17.30 | 17.19 | 17.16 | 17.01 | 16.90 | 16.82 | 16.72 |
| 11  | 0 45 33.87 | 20 24 54.90 | 0.109           | 4   | 20.71 | 20.45 | 20.25 | 19.55 | 19.60 | 19.40 | 19.30 | 19.19 | 18.94 | 19.28 | 18.89 | 18.97 | 18.86 | 18.69 | 18.39 |
| 12  | 0 45 34.15 | 20 42 13.30 | 0.100           | 1   | 21.61 | 21.22 | 20.71 | 20.34 | 19.86 | 19.44 | 19.25 | 19.04 | 18.97 | 18.62 | 18.74 | 18.72 | 18.58 | 18.49 | 18.37 |
| 13  | 0 45 38.09 | 20 39 56.00 | 0.086           | 1   | 22.06 | 21.12 | 20.59 | 20.05 | 19.29 | 18.89 | 18.55 | 18.43 | 18.15 | 18.07 | 17.90 | 17.80 | 17.73 | 17.58 | 17.36 |
| 14  | 0 45 39.48 | 20 18 25.70 | 0.089           | 1   | 21.20 | 21.80 | 20.96 | 20.19 | 19.55 | 19.35 | 19.12 | 18.91 | 18.57 | 18.49 | 18.55 | 18.29 | 18.37 | 18.18 | 17.91 |
| 15  | 0 45 41.68 | 20 34 10.30 | 0.090           | 3   | 19.86 | 19.95 | 19.79 | 18.89 | 18.57 | 18.42 | 18.20 | 18.00 | 17.83 | 17.98 | 17.58 | 17.57 | 17.40 | 17.33 | 17.40 |
| 16  | 0 45 45.13 | 20 36 18.40 | 0.094           | 7   | 20.20 | 20.26 | 20.26 | 19.30 | 19.66 | 19.42 | 19.53 | 19.21 | 19.12 | 19.40 | 19.20 | 18.82 | 18.88 | 19.33 | 18.75 |
| 17  | 0 45 45.64 | 20 43 24.70 | 0.106           | 1   | 20.63 | 20.52 | 20.49 | 19.62 | 19.20 | 18.82 | 18.55 | 18.35 | 18.14 | 18.03 | 17.95 | 17.96 | 17.81 | 17.67 | 17.63 |
| 18  | 0 45 45.90 | 20 44 45.80 | 0.093           | 4   | 20.09 | 19.77 | 19.58 | 18.89 | 18.84 | 18.67 | 18.44 | 18.36 | 18.14 | 18.17 | 18.06 | 17.90 | 17.79 | 17.69 | 17.69 |
| 19  | 0 45 46.09 | 20 23 30.80 | 0.093           | 1   | 20.91 | 19.86 | 19.90 | 18.86 | 18.58 | 18.32 | 18.14 | 17.99 | 17.74 | 17.72 | 17.57 | 17.45 | 17.40 | 17.21 | 17.27 |
| 20  | 0 45 46.13 | 20 28 48.10 | 0.097           | 2   | 20.45 | 20.69 | 20.12 | 19.04 | 18.56 | 18.24 | 18.06 | 17.88 | 17.65 | 17.66 | 17.53 | 17.37 | 17.21 | 17.11 | 16.97 |
| 21  | 0 45 47.17 | 20 29 51.20 | 0.086           | 1   | 20.40 | 19.74 | 19.20 | 18.34 | 18.17 | 18.07 | 17.77 | 17.68 | 17.61 | 17.45 | 17.59 | 17.46 | 17.43 | 17.42 | 17.21 |
| 22  | 0 45 47.30 | 20 26 54.30 | 0.084           | 1   | 18.67 | 17.86 | 17.54 | 16.85 | 16.56 | 16.44 | 16.18 | 16.09 | 15.91 | 15.92 | 15.80 | 15.73 | 15.63 | 15.51 | 15.57 |
| 23  | 0 45 47.44 | 20 34 03.80 | 0.112           | 1   | 21.73 | 20.48 | 20.86 | 19.85 | 19.58 | 19.33 | 19.12 | 18.95 | 18.79 | 18.82 | 18.58 | 18.59 | 18.46 | 18.13 | 18.38 |
| 24  | 0 45 47.95 | 20 36 47.30 | 0.101           | 4   | 21.62 | 20.99 | 24.61 | 20.81 | 20.81 | 20.75 | 20.52 | 20.16 | 20.36 | 20.01 | 20.12 | 20.18 | 20.09 | 19.67 | 18.92 |
| 25  | 0 45 48.35 | 20 43 24.30 | 0.096           | 3   | 21.32 | 20.16 | 20.86 | 19.67 | 19.34 | 19.39 | 19.27 | 18.95 | 18.68 | 18.63 | 18.52 | 18.45 | 18.38 | 18.15 | 18.17 |
| 26  | 0 45 50.74 | 20 18 07.90 | 0.084           | 3   | 20.50 | 19.80 | 19.62 | 18.65 | 18.22 | 18.07 | 17.85 | 17.67 | 17.48 | 17.41 | 17.28 | 17.15 | 17.12 | 16.87 | 16.79 |
| 27  | 0 45 53.08 | 20 12 59.70 | 0.089           | 3   | 20.99 | 20.49 | 20.42 | 19.64 | 19.34 | 19.12 | 18.94 | 18.74 | 18.56 | 18.47 | 18.26 | 18.26 | 18.01 | 18.13 | 17.94 |
| 28  | 0 45 55.14 | 20 26 57.50 | 0.085           | 2   | 20.90 | 19.85 | 19.72 | 18.78 | 18.28 | 17.98 | 17.78 | 17.56 | 17.38 | 17.15 | 17.10 | 16.98 | 16.84 | 16.78 | 16.64 |
| 29  | 0 45 55.17 | 20 29 59.50 | 0.086           | 4   | 19.90 | 20.34 | 19.61 | 18.98 | 18.86 | 18.74 | 18.49 | 18.39 | 18.18 | 18.11 | 17.95 | 17.94 | 17.83 | 17.75 | 17.71 |
| 30  | 0 45 55.67 | 20 28 38.10 | 0.095           | 2   | 20.67 | 19.61 | 19.62 | 18.76 | 18.31 | 18.07 | 17.82 | 17.63 | 17.42 | 17.35 | 17.22 | 17.12 | 16.98 | 16.79 | 16.85 |
| 31  | 0 45 56.39 | 20 43 21.50 | 0.095           | 1   | 20.53 | 19.25 | 19.20 | 18.35 | 17.89 | 17.57 | 17.36 | 17.23 | 17.02 | 16.94 | 16.88 | 16.73 | 16.64 | 16.50 | 16.36 |
| 32  | 0 45 57.54 | 20 37 00.80 | 0.098           | 3   | 19.90 | 19.16 | 18.99 | 18.44 | 18.09 | 17.86 | 17.70 | 17.52 | 17.29 | 17.24 | 17.10 | 16.99 | 16.87 | 16.72 | 16.61 |
| 33  | 0 45 57.59 | 20 36 55.30 | 0.096           | 3   | 19.41 | 18.77 | 18.63 | 17.95 | 17.64 | 17.45 | 17.26 | 17.08 | 16.85 | 16.84 | 16.67 | 16.56 | 16.44 | 16.28 | 16.20 |
| 34  | 0 45 58.53 | 20 29 17.50 | 0.090           | 3   | 21.64 | 20.39 | 20.84 | 19.33 | 19.09 | 19.06 | 18.81 | 18.61 | 18.35 | 18.17 | 18.15 | 18.04 | 17.89 | 17.76 | 17.68 |
| 35  | 0 45 58.54 | 20 21 37.40 | 0.097           | 1   | 20.54 | 20.22 | 20.09 | 19.02 | 18.89 | 18.65 | 18.49 | 18.38 | 18.18 | 18.14 | 18.01 | 17.99 | 17.92 | 17.75 | 17.69 |
| 36  | 0 45 59.60 | 20 17 58.80 | 0.090           | 3   | 20.13 | 20.19 | 19.86 | 18.97 | 18.71 | 18.53 | 18.28 | 18.17 | 17.99 | 17.85 | 17.79 | 17.72 | 17.51 | 17.53 | 17.25 |
| 37  | 0 46 00.13 | 20 20 32.20 | 0.101           | 2   | 21.13 | 20.53 | 20.07 | 19.32 | 18.73 | 18.45 | 18.24 | 18.07 | 17.82 | 17.86 | 17.67 | 17.57 | 17.45 | 17.24 | 17.16 |
| 38  | 0 46 01.41 | 20 30 13.30 | 0.106           | 3   | 20.62 | 21.42 | 20.31 | 19.13 | 18.98 | 18.70 | 18.60 | 18.40 | 18.14 | 18.17 | 17.97 | 17.89 | 17.83 | 17.57 | 17.58 |
| 39  | 0 46 01.76 | 20 21 27.50 | 0.089           | 1   | 18.82 | 18.17 | 18.02 | 17.60 | 17.54 | 17.40 | 17.28 | 17.26 | 17.23 | 17.16 | 17.17 | 17.19 | 17.17 | 17.24 | 17.04 |
| 40  | 0 46 01.81 | 20 36 38.00 | 0.104           | 5   | 20.86 | 20.23 | 20.53 | 19.86 | 19.72 | 19.61 | 19.61 | 19.43 | 19.21 | 19.24 | 19.34 | 19.16 | 19.25 | 19.10 | 18.64 |
| 41  | 0 46 02.73 | 20 36 06.20 | 0.098           | 7   | 19.57 | 19.19 | 19.22 | 18.58 | 18.45 | 18.45 | 18.38 | 18.31 | 18.19 | 18.24 | 18.08 | 18.05 | 17.90 | 17.97 | 17.96 |
| 42  | 0 46 03.37 | 20 28 08.40 | 0.108           | 1   | 21.45 | 20.46 | 19.87 | 19.47 | 19.06 | 18.78 | 18.51 | 18.36 | 18.14 | 18.11 | 18.02 | 17.90 | 17.73 | 17.63 | 17.63 |
| 43  | 0 46 04.88 | 20 43 58.50 | 0.100           | 3   | 21.40 | 20.97 | 20.79 | 20.17 | 20.04 | 19.64 | 19.49 | 19.36 | 19.16 | 19.10 | 18.94 | 18.78 | 18.74 | 18.46 | 18.24 |
| 44  | 0 46 06.64 | 20 25 57.20 | 0.087           | 1   | 19.73 | 19.14 | 18.76 | 18.12 | 17.96 | 17.90 | 17.73 | 17.62 | 17.53 | 17.56 | 17.45 | 17.35 | 17.40 | 17.28 | 17.28 |
| 45  | 0 46 07.55 | 20 28 46.40 | 0.099           | 1   | 20.35 | 19.34 | 19.35 | 18.24 | 17.79 | 17.44 | 17.23 | 17.03 | 16.81 | 16.75 | 16.68 | 16.56 | 16.42 | 16.25 | 16.22 |
| 46  | 0 46 07.73 | 20 28 27.00 | 0.101           | 2   | 20.53 | 20.53 | 20.97 | 19.80 | 19.08 | 18.82 | 18.69 | 18.49 | 18.26 | 18.17 | 18.14 | 18.03 | 17.84 | 17.75 | 17.67 |
| 47  | 0 46 10.80 | 20 40 41.00 | 0.100           | 3   | 18.98 | 18.74 | 18.35 | 17.46 | 17.65 | 16.88 | 16.86 | 16.67 | 16.72 | 15.78 | 16.31 | 16.18 | 16.14 | 16.00 | 15.72 |
| 48  | 0 46 10.92 | 20 37 11.90 | 0.096           | 7   | 19.84 | 19.59 | 19.40 | 18.85 | 19.04 | 18.94 | 18.90 | 18.84 | 18.70 | 18.59 | 18.72 | 18.57 | 18.40 | 18.58 | 18.69 |
| 49  | 0 46 11.16 | 20 22 11.60 | 0.106           | 1   | 20.02 | 19.41 | 19.34 | 18.75 | 18.72 | 18.58 | 18.59 | 18.57 | 18.47 | 18.35 | 18.44 | 18.38 | 18.57 | 18.33 | 17.95 |
| 50  | 0 46 12.59 | 20 26 57.40 | 0.105           | 1   | 19.14 | 18.68 | 18.62 | 18.10 | 18.02 | 17.89 | 17.72 | 17.66 | 17.54 | 17.54 | 17.49 | 17.47 | 17.48 | 17.39 | 17.49 |
| 51  | 0 46 12.71 | 20 30 41.70 | 0.095           | 2   | 20.40 | 19.77 | 19.57 | 18.86 | 18.43 | 18.14 | 17.90 | 17.70 | 17.47 | 17.40 | 17.26 | 17.13 | 17.01 | 16.83 | 16.76 |
| 52  | 0 46 13.48 | 20 19 25.60 | 0.094           | 1   | 18.74 | 18.71 | 18.23 | 16.84 | 17.13 | 16.43 | 16.41 | 16.25 | 16.18 | 14.60 | 16.04 | 15.76 | 15.67 | 16.08 | 15.33 |
| 53  | 0 46 13.55 | 20 36 11.90 | 0.085           | 7   | 19.24 | 19.04 | 18.81 | 18.50 | 18.36 | 18.30 | 18.24 | 18.21 | 18.10 | 18.01 | 18.01 | 17.88 | 17.85 | 17.81 | 17.99 |
| 54  | 0 46 15.10 | 20 29 56.70 | 0.089           | 1   | 21.24 | 20.28 | 20.21 | 19.29 | 18.69 | 18.43 | 18.10 | 17.96 | 17.74 | 17.64 | 17.54 | 17.45 | 17.23 | 17.16 | 17.07 |
| 55  | 0 46 15.40 | 20 44 16.30 | 0.101           | 1   | 22.48 | 21.88 | 22.92 | 20.54 | 20.09 | 19.93 | 19.86 | 19.71 | 19.58 | 19.11 | 19.41 | 19.46 | 19.40 | 19.05 | 18.72 |
| 56  | 0 46 15.70 | 20 32 07.40 | 0.087           | 1   | 20.19 | 19.85 | 19.61 | 18.82 | 18.49 | 18.24 | 17.95 | 17.83 | 17.61 | 17.71 | 17.49 | 17.35 | 17.24 | 17.11 | 17.05 |
| 57  | 0 46 15.97 | 20 30 55.50 | 0.096           | 1   | 20.78 | 19.89 | 19.91 | 19.04 | 19.12 | 18.97 | 18.82 | 18.75 | 18.75 | 18.39 | 18.75 | 18.54 | 18.61 | 18.41 | 18.21 |
| 58  | 0 46 16.25 | 20 32 35.10 | 0.086           | 2   | 21.40 | 20.68 | 20.67 | 19.76 | 19.4  |       |       |       |       |       |       |       |       |       |       |

Table 3 — *Continued.*

| No. | R.A.       | Decl.       | $z_{\text{ph}}$ | $T$ | $a$   | $b$   | $c$   | $d$     | $e$   | $f$   | $g$   | $h$   | $i$   | $j$   | $k$   | $m$   | $n$   | $o$   | $p$   |
|-----|------------|-------------|-----------------|-----|-------|-------|-------|---------|-------|-------|-------|-------|-------|-------|-------|-------|-------|-------|-------|
| 61  | 0 46 17.97 | 20 32 34.60 | 0.096           | 1   | 19.65 | 19.24 | 19.07 | 18.40   | 18.23 | 18.11 | 17.99 | 17.88 | 17.78 | 17.50 | 17.65 | 17.55 | 17.51 | 17.38 | 17.37 |
| 62  | 0 46 18.20 | 20 42 15.90 | 0.092           | 3   | 20.18 | 19.44 | 19.23 | 18.58   | 18.17 | 17.95 | 17.77 | 17.61 | 17.42 | 17.34 | 17.21 | 17.13 | 16.98 | 16.88 | 16.82 |
| 63  | 0 46 18.77 | 20 24 49.10 | 0.109           | 1   | 22.85 | 22.05 | 21.84 | 20.36   | 20.78 | 20.46 | 20.31 | 19.94 | 19.77 | 19.57 | 19.74 | 19.80 | 19.35 | 19.74 | 19.27 |
| 64  | 0 46 20.84 | 20 21 27.30 | 0.085           | 7   | 21.44 | 20.87 | 20.93 | 20.13   | 20.10 | 19.92 | 19.97 | 19.83 | 19.72 | 19.36 | 19.26 | 19.33 | 19.56 | 19.72 | 18.87 |
| 65  | 0 46 20.91 | 20 31 01.10 | 0.088           | 1   | 21.20 | 21.38 | 20.99 | 19.98   | 19.34 | 19.11 | 18.93 | 18.74 | 18.56 | 18.63 | 18.48 | 18.26 | 18.21 | 18.06 | 18.05 |
| 66  | 0 46 21.31 | 20 43 33.80 | 0.087           | 1   | 20.87 | 20.11 | 19.89 | 18.97   | 18.52 | 18.32 | 18.14 | 17.98 | 17.72 | 17.74 | 17.52 | 17.42 | 17.45 | 17.23 | 17.21 |
| 67  | 0 46 22.36 | 20 25 15.50 | 0.110           | 2   | 20.66 | 19.89 | 19.90 | 18.82   | 18.54 | 18.21 | 18.03 | 17.84 | 17.57 | 17.60 | 17.38 | 17.32 | 17.22 | 16.97 | 17.03 |
| 68  | 0 46 22.56 | 20 23 30.00 | 0.082           | 1   | 20.54 | 20.16 | 19.76 | 19.40   | 19.31 | 19.32 | 19.14 | 19.16 | 19.01 | 19.14 | 18.87 | 18.98 | 18.96 | 19.18 | 18.86 |
| 69  | 0 46 22.63 | 20 34 11.40 | 0.101           | 1   | 22.00 | 20.29 | 20.81 | 20.11   | 19.34 | 19.08 | 18.82 | 18.61 | 18.49 | 18.41 | 18.22 | 18.22 | 17.90 | 17.88 | 17.73 |
| 70  | 0 46 23.28 | 20 29 38.90 | 0.090           | 1   | 21.98 | 20.67 | 20.45 | 19.42   | 18.79 | 18.47 | 18.31 | 18.05 | 17.81 | 17.75 | 17.59 | 17.44 | 17.37 | 17.26 | 17.18 |
| 71  | 0 46 23.64 | 20 37 28.40 | 0.097           | 1   | 21.78 | 20.55 | 20.43 | 19.25   | 18.72 | 18.18 | 18.03 | 17.89 | 17.62 | 17.34 | 17.45 | 17.31 | 17.29 | 17.08 | 17.04 |
| 72  | 0 46 24.35 | 20 37 36.30 | 0.087           | 1   | 20.63 | 20.28 | 20.12 | 18.78   | 18.33 | 18.05 | 17.81 | 17.66 | 17.49 | 17.05 | 17.30 | 17.20 | 17.16 | 17.05 | 16.98 |
| 73  | 0 46 24.55 | 20 30 02.50 | 0.096           | 1   | 20.45 | 19.84 | 19.62 | 18.57   | 18.22 | 17.93 | 17.69 | 17.50 | 17.27 | 17.04 | 17.09 | 17.00 | 16.83 | 16.76 | 16.69 |
| 74  | 0 46 24.76 | 20 36 59.00 | 0.085           | 2   | 20.86 | 20.39 | 20.75 | 19.65   | 19.08 | 18.79 | 18.56 | 18.47 | 18.33 | 17.79 | 18.05 | 17.95 | 17.85 | 17.73 | 17.45 |
| 75  | 0 46 25.03 | 20 22 48.50 | 0.106           | 4   | 21.26 | 21.77 | 20.89 | 20.41   | 19.22 | 19.88 | 19.87 | 19.66 | 19.54 | 19.53 | 19.24 | 19.36 | 19.49 | 18.83 | 18.40 |
| 76  | 0 46 25.13 | 20 29 06.60 | 0.097           | 2   | 21.41 | 20.17 | 20.25 | 19.12   | 18.78 | 18.40 | 18.13 | 17.98 | 17.75 | 17.67 | 17.45 | 17.39 | 17.24 | 17.06 | 16.97 |
| 77  | 0 46 25.63 | 20 30 33.80 | 0.105           | 2   | 20.14 | 19.82 | 19.96 | 18.96   | 18.54 | 18.19 | 18.02 | 17.82 | 17.57 | 17.55 | 17.38 | 17.30 | 17.16 | 16.99 | 16.91 |
| 78  | 0 46 26.68 | 20 28 17.40 | 0.106           | 1   | 21.63 | 20.76 | 21.20 | 19.52   | 19.08 | 18.66 | 18.39 | 18.29 | 17.99 | 18.05 | 17.83 | 17.80 | 17.55 | 17.41 | 17.36 |
| 79  | 0 46 26.76 | 20 21 44.70 | 0.086           | 1   | 19.15 | 18.51 | 18.38 | 17.82   | 17.59 | 17.58 | 17.40 | 17.32 | 17.24 | 17.14 | 17.18 | 17.11 | 17.11 | 17.02 | 17.03 |
| 80  | 0 46 27.41 | 20 35 40.00 | 0.090           | 3   | 20.15 | 20.25 | 20.75 | 19.44   | 19.20 | 19.00 | 18.84 | 18.67 | 18.43 | 18.30 | 18.13 | 18.09 | 18.01 | 17.92 | 17.66 |
| 81  | 0 46 27.88 | 20 30 51.60 | 0.094           | 1   | 20.88 | 19.81 | 20.66 | 19.06   | 18.69 | 18.38 | 18.19 | 18.01 | 17.72 | 17.68 | 17.52 | 17.43 | 17.36 | 17.20 | 17.10 |
| 82  | 0 46 28.05 | 20 17 16.70 | 0.093           | 7   | 21.07 | 20.55 | 20.22 | 19.75   | 19.74 | 19.55 | 19.60 | 19.40 | 19.35 | 19.18 | 19.06 | 19.14 | 19.12 | 19.13 | 18.45 |
| 83  | 0 46 28.06 | 20 17 29.00 | 0.090           | 4   | 19.83 | 19.40 | 19.28 | 18.57   | 18.39 | 18.27 | 18.12 | 18.02 | 17.79 | 17.80 | 17.60 | 17.56 | 17.45 | 17.42 | 17.43 |
| 84  | 0 46 28.30 | 20 27 59.80 | 0.086           | 1   | 19.11 | 18.49 | 18.18 | 17.52   | 17.28 | 17.12 | 16.91 | 16.80 | 16.65 | 16.50 | 16.55 | 16.47 | 16.45 | 16.37 | 16.33 |
| 85  | 0 46 28.37 | 20 28 10.70 | 0.098           | 1   | 20.76 | 20.47 | 20.32 | 19.06   | 18.68 | 18.30 | 18.14 | 17.96 | 17.74 | 17.26 | 17.64 | 17.46 | 17.33 | 17.23 | 17.09 |
| 86  | 0 46 28.93 | 20 27 53.80 | 0.101           | 1   | 20.92 | 19.91 | 19.76 | 18.62   | 18.30 | 17.88 | 17.64 | 17.44 | 17.22 | 16.76 | 17.05 | 16.93 | 16.77 | 16.64 | 16.52 |
| 87  | 0 46 29.03 | 20 26 11.80 | 0.105           | 1   | 19.75 | 19.42 | 19.59 | 18.71   | 18.61 | 18.51 | 18.35 | 18.24 | 18.18 | 17.97 | 18.15 | 18.10 | 17.98 | 17.94 | 17.82 |
| 88  | 0 46 29.05 | 20 26 02.90 | 0.110           | 1   | 21.14 | 21.75 | 20.45 | 19.44   | 19.30 | 19.05 | 18.87 | 18.70 | 18.46 | 18.37 | 18.37 | 18.35 | 18.10 | 17.93 | 17.73 |
| 89  | 0 46 29.14 | 20 30 08.00 | 0.099           | 1   | 20.54 | 19.80 | 19.48 | 18.79   | 18.47 | 18.18 | 18.02 | 17.77 | 17.57 | 17.59 | 17.39 | 17.32 | 17.20 | 17.09 | 17.07 |
| 90  | 0 46 29.23 | 20 29 20.80 | 0.100           | 3   | 18.69 | 18.36 | 17.83 | 16.98   | 17.21 | 16.62 | 16.51 | 16.39 | 16.26 | 14.93 | 15.91 | 15.63 | 15.56 | 15.47 | 15.25 |
| 91  | 0 46 29.34 | 20 27 30.20 | 0.108           | 3   | 20.40 | 20.12 | 19.48 | 19.07   | 18.79 | 18.46 | 18.33 | 18.16 | 17.87 | 17.98 | 17.68 | 17.64 | 17.57 | 17.37 | 17.30 |
| 92  | 0 46 29.43 | 20 26 09.50 | 0.106           | 1   | 20.33 | 20.05 | 19.66 | 18.84   | 18.74 | 18.54 | 18.34 | 18.26 | 18.14 | 17.95 | 18.07 | 18.00 | 17.74 | 17.72 | 17.62 |
| 93  | 0 46 29.53 | 20 42 50.60 | 0.098           | 2   | 20.40 | 20.60 | 19.93 | 19.22   | 18.78 | 18.49 | 18.34 | 18.13 | 17.90 | 17.66 | 17.86 | 17.65 | 17.56 | 17.42 | 17.27 |
| 94  | 0 46 29.74 | 20 39 00.30 | 0.096           | 2   | 19.73 | 18.75 | 18.60 | 17.71   | 17.15 | 16.85 | 16.66 | 16.45 | 16.21 | 16.17 | 16.03 | 15.93 | 15.75 | 15.62 | 15.54 |
| 95  | 0 46 29.82 | 20 19 00.40 | 0.096           | 6   | 21.68 | 20.95 | 21.46 | 20.18   | 20.44 | 20.34 | 20.06 | 20.19 | 19.99 | 20.23 | 19.90 | 19.87 | 19.53 | 19.87 | 19.02 |
| 96  | 0 46 29.84 | 20 42 38.80 | 0.093           | 1   | 20.46 | 19.25 | 19.03 | 18.50   | 18.21 | 18.08 | 17.99 | 17.75 | 17.61 | 17.16 | 17.50 | 17.33 | 17.30 | 17.18 | 17.14 |
| 97  | 0 46 30.00 | 20 38 52.10 | 0.110           | 1   | 20.33 | 19.26 | 19.25 | 18.07   | 17.59 | 17.26 | 17.09 | 16.87 | 16.65 | 16.56 | 16.45 | 16.38 | 16.18 | 16.05 | 16.06 |
| 98  | 0 46 30.00 | 20 37 04.40 | 0.088           | 1   | 20.42 | 19.43 | 19.19 | 18.57   | 18.13 | 17.81 | 17.58 | 17.43 | 17.22 | 17.11 | 17.03 | 16.90 | 16.80 | 16.69 | 16.62 |
| 99  | 0 46 30.22 | 20 36 41.20 | 0.094           | 1   | 20.91 | 20.08 | 19.88 | 18.62   | 18.18 | 17.86 | 17.70 | 17.48 | 17.26 | 16.96 | 17.12 | 16.99 | 16.95 | 16.75 | 16.58 |
| 100 | 0 46 30.34 | 20 16 36.40 | 0.091           | 1   | 22.92 | 21.70 | 21.19 | 19.78   | 19.68 | 19.35 | 19.23 | 19.07 | 18.92 | 18.64 | 18.80 | 18.65 | 18.43 | 18.48 | 18.23 |
| 101 | 0 46 30.36 | 20 17 00.30 | 0.096           | 3   | 20.57 | 20.06 | 19.98 | 19.09   | 18.80 | 18.62 | 18.51 | 18.33 | 18.13 | 18.15 | 17.92 | 17.90 | 17.74 | 17.67 | 17.50 |
| 102 | 0 46 30.44 | 20 14 41.50 | 0.097           | 1   | 22.20 | 20.61 | 21.22 | 19.64   | 18.99 | 18.55 | 18.37 | 18.12 | 17.87 | 17.95 | 17.70 | 17.52 | 17.39 | 17.25 | 17.23 |
| 103 | 0 46 30.51 | 20 39 01.00 | 0.094           | 1   | 21.33 | 20.49 | 21.09 | 19.30   | 19.03 | 18.67 | 18.48 | 18.25 | 18.06 | 17.49 | 17.83 | 17.75 | 17.53 | 17.56 | 17.48 |
| 104 | 0 46 30.64 | 20 38 57.70 | 0.094           | 1   | 21.53 | 20.26 | 21.64 | 19.64   | 19.27 | 18.98 | 18.77 | 18.47 | 18.31 | 17.72 | 18.04 | 18.01 | 17.83 | 17.79 | 17.77 |
| 105 | 0 46 31.58 | 20 35 21.70 | 0.094           | 1   | 20.25 | 19.87 | 19.84 | 18.80   | 18.62 | 18.51 | 18.37 | 18.29 | 18.14 | 18.01 | 18.05 | 17.85 | 17.91 | 17.63 | 17.82 |
| 106 | 0 46 31.84 | 20 37 40.00 | 0.091           | 2   | 20.95 | 19.91 | 19.78 | 18.96   | 18.20 | 17.96 | 17.78 | 17.56 | 17.36 | 17.27 | 17.14 | 17.04 | 16.92 | 16.77 | 16.56 |
| 107 | 0 46 32.19 | 20 28 05.80 | 0.101           | 1   | 21.28 | 20.18 | 20.18 | 18.95   | 18.47 | 18.19 | 17.99 | 17.78 | 17.50 | 17.38 | 17.43 | 17.29 | 17.15 | 16.99 | 17.02 |
| 108 | 0 46 32.79 | 20 26 58.70 | 0.094           | 1   | 20.90 | 20.62 | 20.74 | 19.36   | 19.29 | 18.76 | 18.53 | 18.32 | 18.14 | 17.99 | 17.90 | 17.80 | 17.64 | 17.58 | 17.52 |
| 109 | 0 46 33.38 | 20 23 58.30 | 0.094           | 2   | 21.48 | 20.07 | 20.21 | 19.13   | 18.74 | 18.43 | 18.23 | 17.93 | 17.77 | 17.42 | 17.48 | 17.38 | 17.24 | 17.13 | 16.94 |
| 110 | 0 46 34.04 | 20 34 41.60 | 0.087           | 7   | 21.21 | 21.08 | 19.92 | 20.30   | 20.42 | 20.08 | 20.11 | 20.43 | 19.40 | 20.04 | 19.94 | 20.76 | 20.36 | 21.50 | 18.84 |
| 111 | 0 46 34.08 | 20 23 04.20 | 0.094           | 1   | 21.34 | 21.08 | 20.85 | 19.58   | 19.29 | 19.00 | 18.77 | 18.59 | 18.43 | 18.33 | 18.25 | 18.15 | 17.94 | 17.88 | 17.85 |
| 112 | 0 46 34.28 | 20 47 57.70 | 0.107           | 2   | 21.44 | 20.19 | 19.49 | 19.42   | 18.79 | 18.45 | 18.24 | 18.03 | 17.79 | 17.66 | 17.60 | 17.48 | 17.26 | 17.12 | 16.97 |
| 113 | 0 46 34.30 | 20 28 07.40 | 0.094           | 1   | 20.12 | 19.58 | 19.81 | 18.76   | 18.15 | 17.88 | 17.64 | 17.46 | 17.16 | 17.21 | 17.03 | 16.88 | 16.77 | 16.62 | 16.56 |
| 114 | 0 46 34.44 | 20 30 10.80 | 0.092           | 1   | 22.11 | 20.18 | 21.00 | 19.49   | 19.13 | 18.80 | 18.55 | 18.39 | 18.21 | 18.17 | 18.06 | 17.92 | 17.69 | 17.67 | 17.57 |
| 115 | 0 46 34.63 | 20 28 08.40 | 0.094           | 1   | 20.78 | 19.24 | 19.68 | 18.75   | 18.01 | 17.78 | 17.52 | 17.37 | 17.05 | 17.13 | 16.94 | 16.80 | 16.67 | 16.52 | 16.39 |
| 116 | 0 46 35.75 | 20 34 36.60 | 0.100           | 1   | 21.62 | 20.24 | 20.05 | 19.48   | 19.03 | 18.50 | 18.39 | 18.18 | 17.99 | 18.03 | 17.82 | 17.66 | 17.54 | 17.43 | 17.37 |
| 117 | 0 46 35.79 | 20 28 32.30 | 0.100           | 2   | 20.87 | 20.05 | 19.45 | 18.61   | 18.21 | 17.79 | 17.58 | 17.41 | 17.20 | 16.88 | 16.93 | 16.83 | 16.62 | 16.51 | 16.40 |
| 118 | 0 46 36.10 | 20 38 40.20 | 0.093           | 2   | 20.36 | 19.55 | 19.34 | 18.74</ |       |       |       |       |       |       |       |       |       |       |       |

Table 3 — *Continued.*

| No. | R.A.       | Decl.       | $z_{\text{ph}}$ | $T$ | $a$   | $b$   | $c$   | $d$   | $e$   | $f$   | $g$   | $h$   | $i$   | $j$   | $k$   | $m$   | $n$   | $o$   | $p$   |
|-----|------------|-------------|-----------------|-----|-------|-------|-------|-------|-------|-------|-------|-------|-------|-------|-------|-------|-------|-------|-------|
| 121 | 0 46 36.67 | 20 32 31.60 | 0.089           | 3   | 21.02 | 20.31 | 20.86 | 19.69 | 19.44 | 19.18 | 19.02 | 18.88 | 18.69 | 18.73 | 18.55 | 18.34 | 18.29 | 18.18 | 17.98 |
| 122 | 0 46 36.89 | 20 46 23.30 | 0.103           | 3   | 20.73 | 19.75 | 19.27 | 18.74 | 18.25 | 17.98 | 17.76 | 17.61 | 17.39 | 17.30 | 17.21 | 17.10 | 16.98 | 16.76 | 16.76 |
| 123 | 0 46 37.00 | 20 20 45.20 | 0.100           | 4   | 22.37 | 21.30 | 19.75 | 20.01 | 19.77 | 19.51 | 19.52 | 19.32 | 19.00 | 19.10 | 18.75 | 18.87 | 18.65 | 18.72 | 18.35 |
| 124 | 0 46 37.03 | 20 40 04.10 | 0.106           | 3   | 21.47 | 20.48 | 20.89 | 19.94 | 19.80 | 19.50 | 19.39 | 19.10 | 18.89 | 18.79 | 18.54 | 18.65 | 18.62 | 18.17 | 18.02 |
| 125 | 0 46 37.06 | 20 36 31.30 | 0.095           | 3   | 20.09 | 19.65 | 19.42 | 18.62 | 18.38 | 18.19 | 18.04 | 17.88 | 17.69 | 17.46 | 17.50 | 17.36 | 17.24 | 17.11 | 17.16 |
| 126 | 0 46 37.07 | 20 36 36.50 | 0.094           | 3   | 20.09 | 19.27 | 19.06 | 18.41 | 18.11 | 17.90 | 17.78 | 17.61 | 17.39 | 17.27 | 17.17 | 17.06 | 16.97 | 16.81 | 16.77 |
| 127 | 0 46 37.09 | 20 36 41.10 | 0.092           | 3   | 20.70 | 19.35 | 19.46 | 18.79 | 18.41 | 18.24 | 18.09 | 17.94 | 17.69 | 17.61 | 17.42 | 17.35 | 17.25 | 17.12 | 16.99 |
| 128 | 0 46 37.27 | 20 35 37.50 | 0.095           | 3   | 21.00 | 21.64 | 20.43 | 20.23 | 20.23 | 19.60 | 19.54 | 19.35 | 19.17 | 18.97 | 19.17 | 18.85 | 18.67 | 18.85 | 17.88 |
| 129 | 0 46 37.43 | 20 18 18.90 | 0.094           | 1   | 18.34 | 18.42 | 17.80 | 17.09 | 17.56 | 16.84 | 17.19 | 16.80 | 17.13 | 15.10 | 16.87 | 16.60 | 16.43 | 16.90 | 16.28 |
| 130 | 0 46 37.85 | 20 35 35.50 | 0.087           | 3   | 20.59 | 20.30 | 19.89 | 19.13 | 18.94 | 18.56 | 18.37 | 18.22 | 18.07 | 18.18 | 17.89 | 17.73 | 17.65 | 17.55 | 17.31 |
| 131 | 0 46 38.21 | 20 22 54.50 | 0.098           | 1   | 20.04 | 19.17 | 19.02 | 18.16 | 17.47 | 17.53 | 17.29 | 17.13 | 16.90 | 16.82 | 16.73 | 16.66 | 16.49 | 16.38 | 16.36 |
| 132 | 0 46 38.40 | 20 29 38.70 | 0.100           | 1   | 22.39 | 20.84 | 21.84 | 20.25 | 20.17 | 19.65 | 19.63 | 19.22 | 19.01 | 19.40 | 18.97 | 18.80 | 18.78 | 18.64 | 18.35 |
| 133 | 0 46 38.52 | 20 18 28.30 | 0.094           | 1   | 17.78 | 17.61 | 17.23 | 16.41 | 16.75 | 16.28 | 16.14 | 16.09 | 16.04 | 14.66 | 16.07 | 15.81 | 15.78 | 16.14 | 15.50 |
| 134 | 0 46 38.62 | 20 22 45.50 | 0.100           | 1   | 20.58 | 19.55 | 19.52 | 18.54 | 18.17 | 17.79 | 17.63 | 17.44 | 17.22 | 16.96 | 17.06 | 16.96 | 16.81 | 16.71 | 16.64 |
| 135 | 0 46 42.40 | 20 27 55.30 | 0.110           | 1   | 20.38 | 21.00 | 20.28 | 19.25 | 19.19 | 19.16 | 19.00 | 18.93 | 18.74 | 18.92 | 18.69 | 18.65 | 18.61 | 18.41 | 18.36 |
| 136 | 0 46 42.50 | 20 35 11.40 | 0.087           | 1   | 22.61 | 21.74 | 21.41 | 20.17 | 20.04 | 19.88 | 19.86 | 19.64 | 19.30 | 19.42 | 19.24 | 19.09 | 18.90 | 19.42 | 18.72 |
| 137 | 0 46 42.67 | 20 15 18.20 | 0.111           | 1   | 20.94 | 20.16 | 19.89 | 19.33 | 18.87 | 18.44 | 18.29 | 18.17 | 17.91 | 17.86 | 17.77 | 17.68 | 17.59 | 17.38 | 17.25 |
| 138 | 0 46 42.79 | 20 45 04.60 | 0.098           | 2   | 20.90 | 20.68 | 20.60 | 19.34 | 19.00 | 18.65 | 18.46 | 18.25 | 18.00 | 17.94 | 17.85 | 17.71 | 17.61 | 17.42 | 17.28 |
| 139 | 0 46 43.09 | 20 13 46.20 | 0.110           | 1   | 21.85 | 20.34 | 20.48 | 19.46 | 18.91 | 18.63 | 18.59 | 18.31 | 18.04 | 17.96 | 17.93 | 17.87 | 17.69 | 17.54 | 17.44 |
| 140 | 0 46 43.12 | 20 29 45.00 | 0.091           | 3   | 20.98 | 20.03 | 19.46 | 18.84 | 18.48 | 18.22 | 18.01 | 17.89 | 17.64 | 17.51 | 17.43 | 17.32 | 17.22 | 17.07 | 17.02 |
| 141 | 0 46 43.65 | 20 36 20.70 | 0.096           | 2   | 20.20 | 19.72 | 19.73 | 18.82 | 18.58 | 18.47 | 18.34 | 18.11 | 17.97 | 17.97 | 17.86 | 17.81 | 17.77 | 17.61 | 17.51 |
| 142 | 0 46 44.27 | 20 27 03.50 | 0.108           | 3   | 20.55 | 20.39 | 20.12 | 19.42 | 19.06 | 18.84 | 18.65 | 18.53 | 18.22 | 18.26 | 18.04 | 17.98 | 17.83 | 17.65 | 17.54 |
| 143 | 0 46 44.28 | 20 18 00.50 | 0.084           | 1   | 18.92 | 18.25 | 17.74 | 16.93 | 16.75 | 16.64 | 16.30 | 16.22 | 16.06 | 16.00 | 15.94 | 15.84 | 15.81 | 15.74 | 15.71 |
| 144 | 0 46 44.43 | 20 18 12.40 | 0.086           | 2   | 21.67 | 21.81 | 20.48 | 20.09 | 19.53 | 19.20 | 19.03 | 18.80 | 18.62 | 17.91 | 18.50 | 18.24 | 18.21 | 18.14 | 17.90 |
| 145 | 0 46 45.62 | 20 35 19.80 | 0.096           | 1   | 22.06 | 21.13 | 20.48 | 19.88 | 19.51 | 19.35 | 19.10 | 19.01 | 18.77 | 18.76 | 18.61 | 18.63 | 18.47 | 18.39 | 18.16 |
| 146 | 0 46 45.88 | 20 37 25.70 | 0.094           | 3   | 20.19 | 20.43 | 20.93 | 19.37 | 19.42 | 18.90 | 18.80 | 18.63 | 18.41 | 18.09 | 18.10 | 17.94 | 17.78 | 17.81 | 17.58 |
| 147 | 0 46 46.55 | 20 28 32.00 | 0.101           | 6   | 19.73 | 19.36 | 19.29 | 18.77 | 18.65 | 18.53 | 18.41 | 18.29 | 18.13 | 18.21 | 17.97 | 17.93 | 17.90 | 17.69 | 17.74 |
| 148 | 0 46 47.53 | 20 28 52.00 | 0.095           | 7   | 20.04 | 20.11 | 19.59 | 19.16 | 19.53 | 19.17 | 19.17 | 19.10 | 18.99 | 19.18 | 18.78 | 18.82 | 19.21 | 18.79 | 18.92 |
| 149 | 0 46 47.61 | 20 30 47.60 | 0.094           | 2   | 21.49 | 20.44 | 20.61 | 19.09 | 18.77 | 18.42 | 18.21 | 18.06 | 17.82 | 17.63 | 17.61 | 17.54 | 17.38 | 17.30 | 16.96 |
| 150 | 0 46 48.01 | 20 22 44.90 | 0.091           | 2   | 21.48 | 20.31 | 20.54 | 19.48 | 19.16 | 18.81 | 18.60 | 18.60 | 18.38 | 18.27 | 18.06 | 18.03 | 17.94 | 17.73 | 17.72 |
| 151 | 0 46 48.52 | 20 15 06.50 | 0.094           | 1   | 19.95 | 19.38 | 19.14 | 18.40 | 18.20 | 18.07 | 17.93 | 17.82 | 17.67 | 17.70 | 17.55 | 17.50 | 17.37 | 17.31 | 17.32 |
| 152 | 0 46 48.57 | 20 29 45.50 | 0.087           | 1   | 20.15 | 19.36 | 19.25 | 18.81 | 18.62 | 18.60 | 18.47 | 18.44 | 18.29 | 18.43 | 18.33 | 18.29 | 18.35 | 18.23 | 18.03 |
| 153 | 0 46 48.69 | 20 31 24.70 | 0.100           | 2   | 20.39 | 19.89 | 19.87 | 18.88 | 18.43 | 18.17 | 17.99 | 17.77 | 17.53 | 17.43 | 17.30 | 17.21 | 17.01 | 16.87 | 16.88 |
| 154 | 0 46 48.82 | 20 15 08.00 | 0.090           | 1   | 20.02 | 19.56 | 19.14 | 18.45 | 18.29 | 18.15 | 17.95 | 17.90 | 17.74 | 17.69 | 17.61 | 17.55 | 17.41 | 17.38 | 17.41 |
| 155 | 0 46 49.03 | 20 25 37.60 | 0.082           | 1   | 21.33 | 21.23 | 20.40 | 19.64 | 19.26 | 19.18 | 18.94 | 18.93 | 18.64 | 18.73 | 18.43 | 18.37 | 18.32 | 18.15 | 18.20 |
| 156 | 0 46 49.30 | 20 28 10.70 | 0.100           | 2   | 20.51 | 20.86 | 20.51 | 19.58 | 19.57 | 19.00 | 18.75 | 18.60 | 18.37 | 18.41 | 18.18 | 18.07 | 18.04 | 17.80 | 17.62 |
| 157 | 0 46 49.68 | 20 28 10.30 | 0.098           | 3   | 20.95 | 21.37 | 20.06 | 19.77 | 19.99 | 19.35 | 19.12 | 18.97 | 18.72 | 19.15 | 18.54 | 18.46 | 18.42 | 18.31 | 17.98 |
| 158 | 0 46 49.70 | 20 43 22.00 | 0.096           | 2   | 19.90 | 19.21 | 18.96 | 18.40 | 18.35 | 18.10 | 17.97 | 17.93 | 17.72 | 17.63 | 17.58 | 17.53 | 17.42 | 17.42 | 17.28 |
| 159 | 0 46 49.97 | 20 28 35.90 | 0.101           | 2   | 20.54 | 20.11 | 19.90 | 19.00 | 18.69 | 18.37 | 18.18 | 18.01 | 17.79 | 17.46 | 17.64 | 17.53 | 17.41 | 17.25 | 17.09 |
| 160 | 0 46 50.02 | 20 20 25.90 | 0.084           | 2   | 21.23 | 20.27 | 20.51 | 19.67 | 19.20 | 19.05 | 19.02 | 18.68 | 18.56 | 18.52 | 18.39 | 18.19 | 18.22 | 18.13 | 18.04 |
| 161 | 0 46 50.39 | 20 20 35.50 | 0.087           | 2   | 20.68 | 20.93 | 20.71 | 19.73 | 19.47 | 19.26 | 19.01 | 18.75 | 18.55 | 18.34 | 18.32 | 18.20 | 18.11 | 18.02 | 17.93 |
| 162 | 0 46 50.59 | 20 45 35.90 | 0.093           | 2   | 19.75 | 19.36 | 18.76 | 18.50 | 18.42 | 18.23 | 18.16 | 18.08 | 17.92 | 18.04 | 17.75 | 17.78 | 17.74 | 17.62 | 17.57 |
| 163 | 0 46 51.33 | 20 15 46.20 | 0.086           | 1   | 20.19 | 19.54 | 19.11 | 18.33 | 18.15 | 18.00 | 17.62 | 17.55 | 17.37 | 17.33 | 17.26 | 17.18 | 17.15 | 17.01 | 16.97 |
| 164 | 0 46 52.00 | 20 41 29.80 | 0.092           | 4   | 22.06 | 22.41 | 21.32 | 20.33 | 20.09 | 20.02 | 20.09 | 19.77 | 19.56 | 19.30 | 19.56 | 19.31 | 19.35 | 19.28 | 18.49 |
| 165 | 0 46 52.98 | 20 21 48.00 | 0.105           | 1   | 20.79 | 20.53 | 20.40 | 19.46 | 19.45 | 19.37 | 19.21 | 19.21 | 19.04 | 19.38 | 19.04 | 19.06 | 19.04 | 18.98 | 18.59 |
| 166 | 0 46 53.04 | 20 29 39.20 | 0.110           | 3   | 21.74 | 23.59 | 24.08 | 21.51 | 21.35 | 21.12 | 21.96 | 20.80 | 20.49 | 21.17 | 21.20 | 20.48 | 20.77 | 20.16 | 19.43 |
| 167 | 0 46 53.08 | 20 29 54.80 | 0.106           | 1   | 21.71 | 22.18 | 21.01 | 20.67 | 20.40 | 20.26 | 20.09 | 20.35 | 19.92 | 19.47 | 19.91 | 20.14 | 20.11 | 19.39 | 19.10 |
| 168 | 0 46 55.60 | 20 34 34.60 | 0.092           | 1   | 22.10 | 20.75 | 20.41 | 19.89 | 19.21 | 18.91 | 18.76 | 18.57 | 18.39 | 18.22 | 18.23 | 18.08 | 17.95 | 17.89 | 17.81 |
| 169 | 0 46 55.88 | 20 28 44.80 | 0.094           | 1   | 20.85 | 19.29 | 19.46 | 18.41 | 17.89 | 17.61 | 17.42 | 17.22 | 17.01 | 16.94 | 16.83 | 16.71 | 16.58 | 16.45 | 16.36 |
| 170 | 0 46 57.48 | 20 28 37.60 | 0.100           | 2   | 21.35 | 21.20 | 20.28 | 19.46 | 19.06 | 18.77 | 18.65 | 18.36 | 18.18 | 18.03 | 17.90 | 17.90 | 17.79 | 17.54 | 17.40 |
| 171 | 0 46 58.32 | 20 37 57.80 | 0.089           | 1   | 20.42 | 19.97 | 19.79 | 19.40 | 19.45 | 19.25 | 19.13 | 19.16 | 19.14 | 19.08 | 19.13 | 19.02 | 19.08 | 19.18 | 18.80 |
| 172 | 0 47 05.18 | 20 38 27.40 | 0.090           | 1   | 20.19 | 19.26 | 19.38 | 18.33 | 17.85 | 17.59 | 17.40 | 17.21 | 17.00 | 16.93 | 16.80 | 16.71 | 16.60 | 16.48 | 16.43 |
| 173 | 0 47 13.04 | 20 35 34.20 | 0.110           | 3   | 21.05 | 20.14 | 20.63 | 19.75 | 19.41 | 19.07 | 18.99 | 18.74 | 18.54 | 18.30 | 18.39 | 18.29 | 18.24 | 17.90 | 18.05 |
| 174 | 0 47 14.30 | 20 33 10.00 | 0.090           | 1   | 21.15 | 20.97 | 21.04 | 19.60 | 19.49 | 19.42 | 19.15 | 19.14 | 18.97 | 18.94 | 18.76 | 18.84 | 18.77 | 18.67 | 18.53 |
| 175 | 0 47 14.44 | 20 17 55.70 | 0.087           | 1   | 20.04 | 19.67 | 19.23 | 18.40 | 18.18 | 18.13 | 17.84 | 17.71 | 17.59 | 17.48 | 17.45 | 17.43 | 17.38 | 17.31 | 17.14 |
| 176 | 0 47 15.15 | 20 37 12.40 | 0.090           | 1   | 20.79 | 20.24 | 19.94 | 19.37 | 19.13 | 18.90 | 18.86 | 18.75 | 18.64 | 18.29 | 18.33 | 18.39 | 18.21 | 18.31 | 17.95 |
| 177 | 0 47 15.19 | 20 17 54.90 | 0.100           | 2   | 20.68 | 20.63 | 20.96 | 19.92 | 19.57 | 19.09 | 18.91 | 18.67 | 18.51 | 18.08 | 18.34 | 18.23 | 18.11 | 17.98 | 17.70 |
| 178 | 0 47 15.45 | 20 26 06.40 | 0.087           |     |       |       |       |       |       |       |       |       |       |       |       |       |       |       |       |

**Table 3** — *Continued.*

| No. | R.A.       | Decl.       | $z_{\text{ph}}$ | $T$ | $a$   | $b$   | $c$   | $d$   | $e$   | $f$   | $g$   | $h$   | $i$   | $j$   | $k$   | $m$   | $n$   | $o$   | $p$   |
|-----|------------|-------------|-----------------|-----|-------|-------|-------|-------|-------|-------|-------|-------|-------|-------|-------|-------|-------|-------|-------|
| 181 | 0 47 15.78 | 20 36 02.70 | 0.105           | 2   | 20.93 | 20.34 | 21.09 | 20.66 | 19.60 | 19.41 | 19.28 | 18.91 | 18.73 | 18.50 | 18.80 | 18.53 | 18.40 | 18.22 | 18.13 |
| 182 | 0 47 16.11 | 20 37 00.10 | 0.097           | 3   | 20.86 | 20.99 | 20.14 | 19.34 | 19.01 | 18.71 | 18.59 | 18.37 | 18.21 | 17.79 | 17.94 | 17.87 | 17.75 | 17.58 | 17.49 |
| 183 | 0 47 16.39 | 20 24 44.60 | 0.092           | 1   | 19.97 | 19.15 | 18.96 | 18.11 | 17.70 | 17.26 | 17.03 | 16.93 | 16.72 | 16.60 | 16.62 | 16.38 | 16.34 | 16.21 | 16.10 |
| 184 | 0 47 19.13 | 20 38 03.90 | 0.096           | 1   | 20.32 | 19.47 | 19.52 | 18.59 | 18.32 | 18.00 | 17.74 | 17.62 | 17.41 | 17.34 | 17.18 | 17.13 | 16.99 | 16.83 | 16.84 |
| 185 | 0 47 20.07 | 20 20 33.60 | 0.095           | 1   | 21.69 | 21.19 | 20.46 | 20.40 | 20.48 | 20.07 | 20.32 | 20.17 | 19.99 | 19.61 | 19.78 | 19.98 | 20.17 | 20.23 | 19.51 |
| 186 | 0 47 20.25 | 20 37 59.50 | 0.100           | 3   | 20.41 | 19.77 | 19.65 | 18.98 | 18.75 | 18.55 | 18.46 | 18.23 | 18.00 | 18.02 | 17.73 | 17.77 | 17.65 | 17.54 | 17.34 |
| 187 | 0 47 22.08 | 20 33 14.50 | 0.110           | 5   | 20.02 | 19.70 | 19.51 | 19.10 | 19.08 | 18.87 | 18.85 | 18.79 | 18.75 | 18.60 | 18.65 | 18.61 | 18.66 | 18.46 | 18.46 |
| 188 | 0 47 25.93 | 20 33 08.50 | 0.090           | 2   | 20.58 | 20.57 | 20.00 | 19.33 | 19.17 | 19.09 | 18.81 | 18.63 | 18.46 | 18.51 | 18.56 | 18.47 | 18.44 | 18.32 | 18.13 |
| 189 | 0 47 26.79 | 20 29 36.40 | 0.106           | 3   | 19.88 | 19.39 | 19.44 | 18.48 | 18.35 | 18.24 | 18.06 | 18.00 | 17.81 | 17.73 | 17.63 | 17.67 | 17.52 | 17.39 | 17.39 |
| 190 | 0 47 26.90 | 20 29 40.40 | 0.101           | 4   | 19.68 | 19.29 | 19.20 | 18.39 | 18.25 | 18.10 | 17.94 | 17.83 | 17.65 | 17.58 | 17.37 | 17.41 | 17.27 | 17.09 | 17.16 |
| 191 | 0 47 27.72 | 20 28 00.60 | 0.094           | 1   | 20.43 | 19.70 | 19.72 | 18.65 | 18.41 | 18.12 | 17.97 | 17.75 | 17.58 | 17.32 | 17.39 | 17.30 | 17.19 | 17.08 | 17.00 |
| 192 | 0 47 28.08 | 20 27 54.10 | 0.097           | 2   | 19.36 | 18.61 | 18.64 | 17.71 | 17.37 | 17.15 | 16.93 | 16.78 | 16.55 | 16.46 | 16.37 | 16.30 | 16.16 | 16.03 | 15.94 |
| 193 | 0 47 28.38 | 20 27 49.60 | 0.094           | 1   | 19.79 | 19.06 | 18.99 | 18.08 | 17.72 | 17.50 | 17.27 | 17.16 | 16.92 | 16.80 | 16.72 | 16.67 | 16.54 | 16.38 | 16.38 |
| 194 | 0 47 35.16 | 20 34 40.90 | 0.086           | 5   | 19.85 | 19.62 | 19.36 | 18.88 | 18.85 | 18.79 | 18.67 | 18.72 | 18.48 | 18.61 | 18.43 | 18.31 | 18.21 | 18.34 | 18.17 |
| 195 | 0 47 36.48 | 20 33 34.30 | 0.108           | 1   | 21.21 | 21.15 | 21.02 | 20.13 | 19.56 | 19.20 | 18.96 | 18.71 | 18.41 | 18.43 | 18.17 | 18.09 | 17.87 | 17.72 | 17.50 |
| 196 | 0 47 39.75 | 20 35 57.10 | 0.083           | 1   | 19.32 | 18.46 | 18.43 | 18.11 | 18.00 | 17.96 | 17.88 | 17.86 | 17.80 | 17.84 | 17.72 | 17.78 | 17.83 | 17.77 | 17.62 |
| 197 | 0 47 40.64 | 20 33 36.70 | 0.087           | 1   | 19.59 | 18.94 | 18.70 | 18.17 | 17.98 | 17.95 | 17.77 | 17.70 | 17.53 | 17.36 | 17.41 | 17.35 | 17.33 | 17.29 | 17.26 |
| 198 | 0 47 43.38 | 20 32 35.00 | 0.090           | 1   | 20.46 | 20.04 | 19.71 | 19.23 | 18.87 | 18.87 | 18.78 | 18.61 | 18.49 | 17.94 | 18.31 | 18.33 | 18.28 | 18.23 | 18.08 |

also marked with filled triangles. Figure 8(a) shows that the 74 bright member galaxies of A98 seem to deviate from a spherically symmetric distribution. The contour map of surface density appears elongated in the north–south direction. Two X-ray peaks are found to be associated with the surface density substructures A98N and A98S. Previous spectroscopy shows that the subcluster A98N is much poorer than the main concentration A98S, which is remarkable in Figure 8(a). Our BATC multicolor photometry facilitates the finding of a large number of faint member galaxies around the northern subcluster A98N, which makes the northern substructure in the surface density more remarkable (see Fig. 8(b)).

What we should keep in mind is that the surface density of A98N is still lower than that of A98S, even after we take all the faint member galaxies into account. However, the northern subcluster A98N is brighter than the southern A98S in the X-ray emission. Forman et al. (1981) reported that the flux ratio between A98N and A98S is about 3:2. Henry et al. (1981) derived a ratio of X-ray luminosity between A98N and A98S of 1.3:1. Considering the contribution to X-ray surface brightness of the central galaxy 0043+2020, KK95 fitted it with the  $\beta$  model, and obtained a lower X-ray luminosity ratio of 1.1:1.

Apart from the northern subcluster A98N, a western subcluster can be seen in Figure 8, at about 12 arcmin west of A98S. This subcluster has not been mentioned before, and we refer to it as A98W. After adding 198 photometrically selected galaxies, Figure 8(b) shows that A98N appears more significant and the western clump A98W still exists. In general, the projected position distribution of the galaxies in sample II is consistent with that of the bright galaxies in sample I.

## 5.2 Localized Velocity Structure

However, the clumps mentioned above might be an enhancement simply due to the projection effect. If a cluster merger occurs along the direction with a definite projection angle, say  $\alpha > 20^\circ$ , with respect to the plane of sky, the substructures can be detected by mapping the localized variation in velocity distribution (Colless & Dunn 1996). The  $\kappa$ -test defines a test statistic  $\kappa_n$  to characterize the local deviation on the scale of groups of  $n$  nearest neighbors.

To detect the substructures in A98, we perform the  $\kappa$ -test for the galaxies in samples I and II. For sample I, there is no significant substructure detected in the localized velocity. We performed  $10^3$  simulations to estimate the probability  $P(\kappa_n > \kappa_n^{\text{obs}})$  in all cases. The probability  $P(\kappa_n > \kappa_n^{\text{obs}})$  is

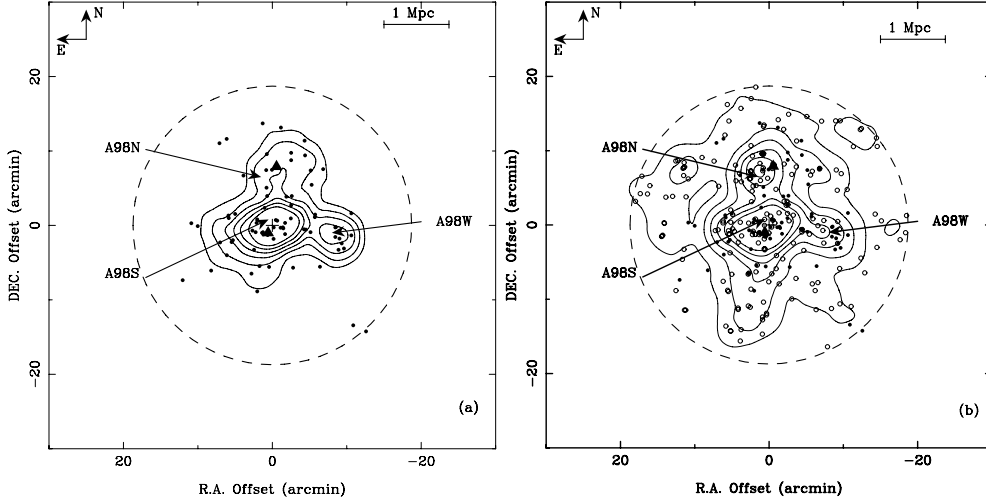


**Fig. 8** *Left* (a): Positions of 74 spectroscopic member galaxies of A98 in sample I. The surface density is smoothed with a Gaussian window of  $\sigma = 1.6'$ . A contour map is superimposed with surface density levels 0.09, 0.15, 0.21, 0.27, 0.33, and  $0.39 \text{ arcmin}^{-2}$ . The dashed circle means a typical region of rich clusters with an Abell radius of  $1.5 h^{-1} \text{ Mpc}$ . Two X-ray peaks are marked with filled triangles. *Right* (b): Position distribution of the 272 member galaxies in sample II, including 74 spectroscopically confirmed member galaxies (*filled circles*) and 198 newly-selected galaxies (*open circles*). A contour map of the surface density for these galaxies is also given with contour levels 0.13, 0.28, 0.43, 0.58, 0.73, and  $0.88 \text{ arcmin}^{-2}$ .

**Table 4** Result of  $\kappa$ -Test for 74 Spectroscopically Confirmed Member Galaxies

| Neighbor size $n$                         | 3    | 4   | 5   | 6    | 7    | 8    | 9    |
|---|------|-----|-----|------|------|------|------|
| $P(\kappa_n > \kappa_n^{\text{obs}})(\%)$ | 11.4 | 5.3 | 9.2 | 14.4 | 16.6 | 24.9 | 40.6 |

found to be more than 5% in a wide range of neighborhood sizes, which means that no substructure is detected at  $2\sigma$  significance. Table 4 gives the result of our  $\kappa$ -test for the galaxies in sample I. However, for the enlarged sample of 272 member galaxies, the probability of substructure detection is greater. Considering the larger relative error in photometric redshift determination, the probability estimate of sample II might be untrue.

Bubble plots in Figure 9 show the localized velocity variation for sample I and sample II using 6 nearest neighbors. The bubble size for each galaxy is proportional to  $-\log[P_{\text{KS}}(D > D_{\text{obs}})]$ . For the galaxies in sample I (see Fig. 9(a)), there are indeed bunches of bubbles at the positions of subcluster A98S and A98W, though the bubble sizes are not very large. A close comparison between Figure 8(a) and Figure 9(a) indicates that A98S and A98W are not simply due to the projection effect: they are most likely real substructures. On the other hand, no bubble clustering is found for the northern subcluster A98N. This seems to support the two-body model where we are looking at a cluster merger between A98N and A98S occurring largely in the plane of the sky, which is consistent with the small projection angle derived in KK95.

For the galaxies in sample II (see Fig. 9(b)), the clustering of bubbles at A98N is enhanced. Taking the faint member galaxies into account, the localized velocity variation between A98S and A98N appears more remarkable. Within the central regions of A98N and A98S, defined by the con-

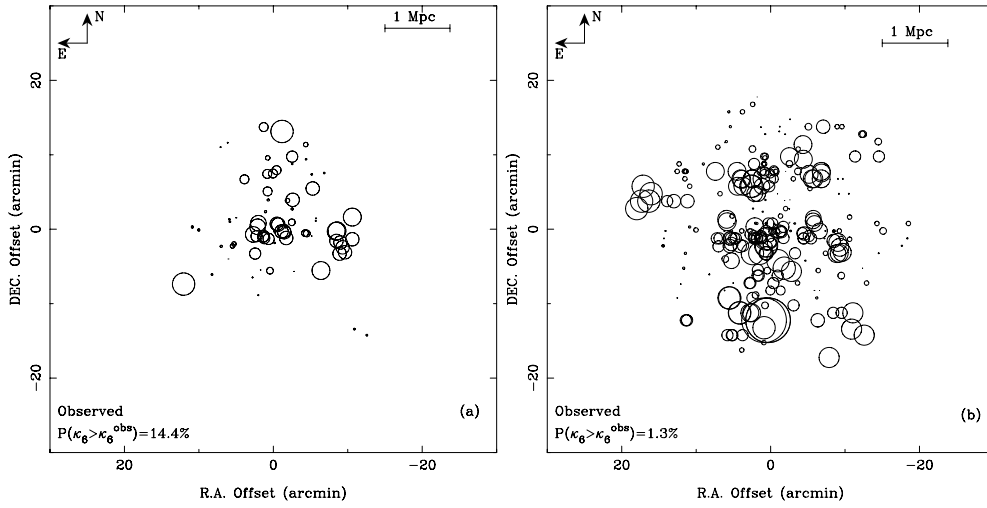


**Fig. 9** (a) Bubble plot for 74 spectroscopic member galaxies of A98. It shows localized variation for groups of the six nearest neighbors. (b) Bubble plot for all the 272 member galaxies of A98 with the same group size as panel (a).

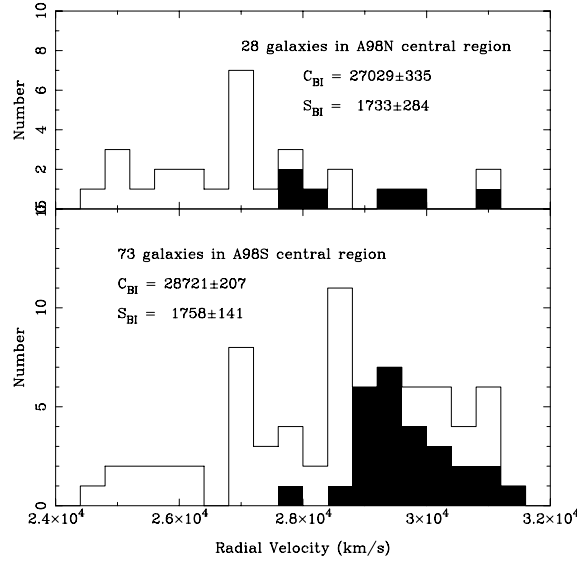


**Fig. 10** Velocity distribution of the galaxies in the central regions of A98N and A98S, defined by the contour curve at  $0.58 \text{ arcmin}^{-2}$  in Fig. 8(b). The velocity distributions of the galaxies in spectroscopic subsamples are shown by shaded histograms.

tour curve at  $0.58 \text{ arcmin}^{-2}$  in Figure 8(b), there are 28 and 73 galaxies, respectively. For the 28 galaxies in A98N, the biweight location is  $27029 \pm 335 \text{ km s}^{-1}$ . However, for the 73 galaxies in A98S, we obtain a higher biweight location,  $28721 \pm 207 \text{ km s}^{-1}$ . The difference in radial velocity between A98N and A98S is about  $1692 \pm 394 \text{ km s}^{-1}$ , which is larger than the typical velocity dispersion of a rich cluster. Figure 10 gives the distributions of radial velocities for these galaxies.

The large velocity difference seems to be a challenge for the bound system. It is noteworthy that the photometric redshifts for the faint member galaxies have a lower precision, and it is necessary to verify the inertial dynamics between A98N and A98S by follow-up deep spectroscopic observations. There are only 6 and 27 galaxies with known  $z_{\text{sp}}$  values within the central regions of A98N and A98S, respectively, for which the velocity distributions are shown in the shaded histograms in Figure 10. For the spectroscopic subsamples in the central regions of A98N and A98S, the biweight locations are 28943 and 29609  $\text{km s}^{-1}$ , respectively. The velocity difference becomes about 666  $\text{km s}^{-1}$ , much smaller than the value of the enlarged samples, which supports the gravitationally bound nature of these two subclusters.

### 5.3 Star Formation Properties

Undoubtedly, the star formation histories of the member galaxies may shed some light on the evolution of their host cluster. With the evolutionary synthesis model, PEGASE (version 2.0, Fioc & Rocca-Volmerange 1997, 1999), we study the star formation properties of A98. Assuming a Salpeter (1955) initial mass function (IMF) and a star formation rate (SFR) in exponentially decreasing form,  $\text{SFR}(t) \propto e^{-t/\tau}$ , where the time scale  $\tau$  ranges from 0.5 to 30.0 Gyr. In order to avoid degeneracy between age and metallicity in the model, we adopt the same age of 12.2 Gyr, corresponding to the age of first generation stars at  $z = 0.104$ , for all member galaxies in A98. A zero initial metallicity of the interstellar medium (ISM) is taken. As a result, a series of rest-frame modeled spectra with various star formation histories is generated by running the PEGASE code, and then they are redshifted to the observer's frame for a given spectroscopic redshift. Convolved with the transmission functions of all the BATC filters, the template SED library for the BATC multicolor photometric system (i.e., relative apparent magnitudes at 15 BATC filters) can be obtained.

Based on the template SED library, we search for the best fit (in the  $\chi^2$  sense) of the observed SEDs of 74 member galaxies with known spectroscopic redshifts. The SFR time scale ( $\tau$ ), mean ISM metallicity ( $Z_{\text{ISM}}$ ), and mean stellar age ( $t_*$ ) can be derived for each bright galaxy. Figure 11 presents the star formation properties as a function of the local surface density,  $\Sigma$ , which is defined by the number of galaxies within an area with a radius of 2.5 arcmin. It is clear in Figure 11 that the star formation properties of the member galaxies in A98 are found to be dependent upon the local density. Panel (a) shows that the galaxies in the outer region are likely to have longer SFR time scales than those in the core region. Considering that late-type galaxies tend to have longer time scales of star formation, our result is consistent with the morphology–density relation first pointed out by Dressler (1980), which can be explained well in the context of the hierarchical cosmological scenario (Poggianti 2004). As shown in the panels (c) and (d), the outlier member galaxies are likely to possess younger stellar populations, resulting in a smaller mean stellar age weighted by either mass or light.

Figure 11(b) gives the variation of the mean ISM metallicities with their local densities. The outlier galaxies have a higher probability of having a lower mean ISM metallicity. It is considered that the galaxies in the core region tend to be more massive and luminous. The underlying physical correlation that allows interpretation of Figure 11(b) is the luminosity–metallicity relation (Lequeux et al. 1979; Melbourne & Salzer 2002) and the mass–metallicity relation (e.g., Garnett & Shields 1987; Tremonti et al. 2004). Figure 12 gives the SFR time scales  $\tau$  and the mean ISM metallicities as functions of the magnitude in the  $h$  band. As all galaxies in A98 have the same distance modulus, the apparent magnitudes could reflect their intrinsic luminosities. For bright and massive cluster galaxies in the core region of A98, their star formation activities have been reduced by some physical processes via environmental effects, such as galaxy–galaxy interaction, harassment, gas stripping, or strangulation (Poggianti 2004; Yuan et al. 2005), which leads to a short SFR time scale. From Figure 11(b) and Figure 12(b), no bright ( $m_h < 16.5$ ) and no central ( $\Sigma > 0.4 \text{ gal. arcmin}^{-2}$ ) galaxies are found to have a mean ISM metallicity less than 0.035, which is consistent with the

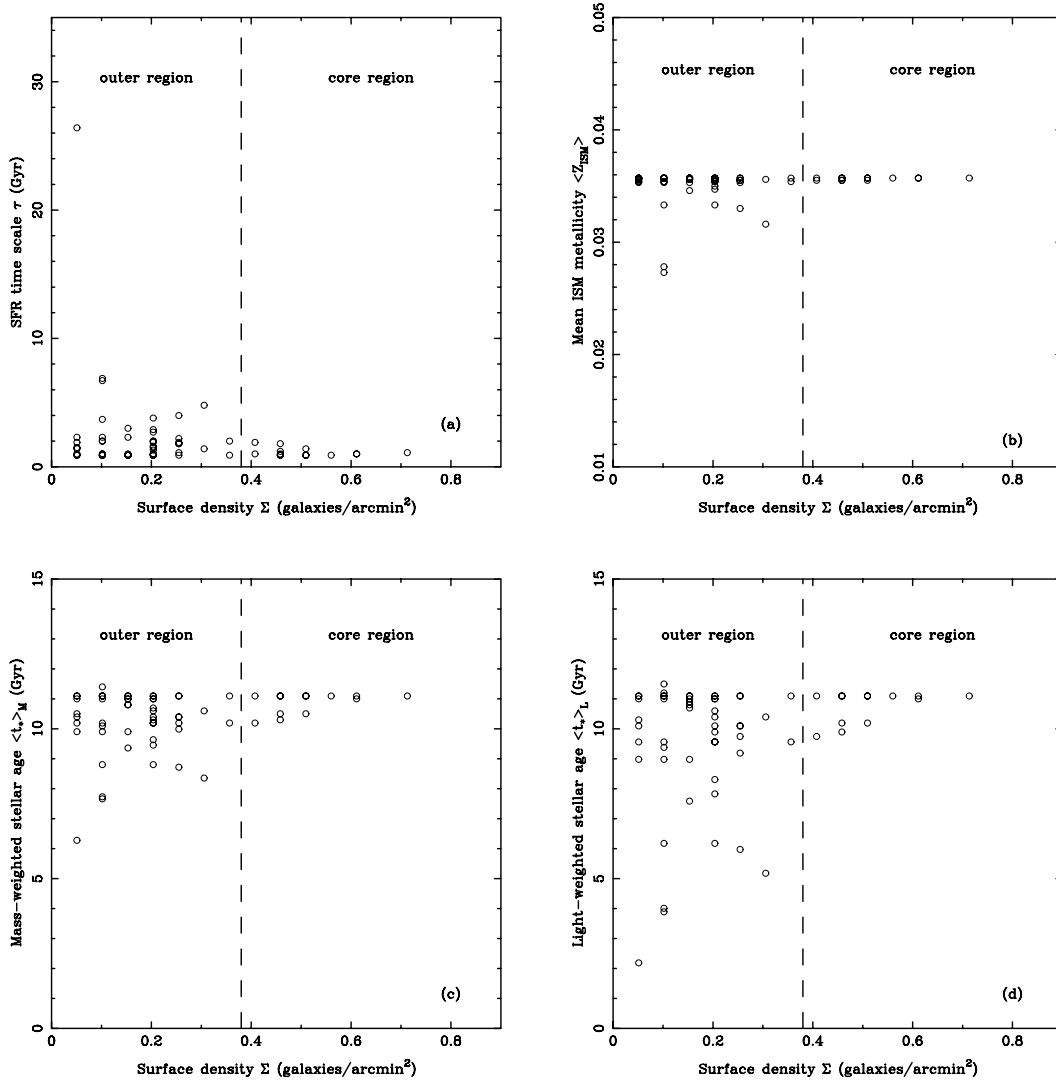


**Fig. 11** Star formation properties for the galaxies with known  $z_{\text{sp}}$  in A98 as functions of local surface density  $\Sigma$ . The star formation properties include the SFR time scale  $\tau$ , metallicity, and the mean stellar ages weighted by mass and light.

ideas that more massive galaxies form fractionally more stars in a Hubble time than their low-mass counterparts, and that metals are selectively lost from faint galaxies with shallow potential wells via galactic winds (Tremonti et al. 2004).

We also tried to find any trends in the property of star formation along the distance from the main concentration of A98. However, no significant environmental effect was found, indicating that A98 is a dynamically complex cluster, and the clustercentric distance is not a good environmental indicator. An alternative explanation is that star formation activities of galaxies in a cluster with ongoing merger events might be more sensitive to galaxy-scale gravitational interactions, not to the cluster-scale environment.

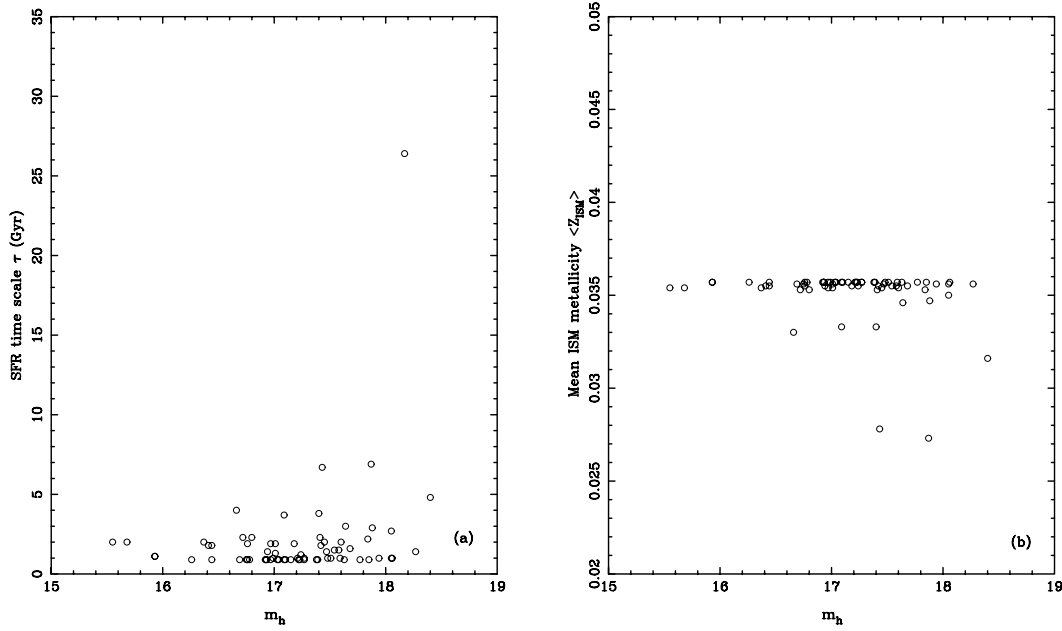


**Fig. 12** The SFR time scales  $\tau$  and mean ISM metallicities for the galaxies with known  $z_{\text{sp}}$  in A98 as functions of magnitude in the  $h$  band.

## 6 SUMMARY

A98 is a galaxy cluster with two large enhancements in X-ray surface brightness. This paper presents our optical photometric observation of A98 with the Beijing–Arizona–Taiwan–Connecticut (BATC) multicolor system. About 8,100 sources are detected down to  $V \sim 20$  mag in a field of  $58' \times 58'$  centered at this cluster, and their spectral energy distributions (SEDs) in 15 intermediate bands are obtained. There are 122 galaxies with spectroscopic redshifts in our field, among which 74 galaxies with  $0.095 < z_{\text{sp}} < 0.115$  are selected as members of A98. The dynamics of two substructures (A98N and A98S) are investigated with the help of the spectroscopic redshifts and the X-ray imaging data. A significant substructure, A98W, is found 10 arcmin to the west of A98S. Within our viewing field, a group of galaxies, A98X, which contains 21 galaxies with  $z_{\text{sp}} \sim 0.120$ , is located  $\sim 15$  arcmin south of A98S. According to the Newtonian gravitational binding criterion, A98X seems to be a separate system which is gravitationally unbound to A98.

After the star-galaxy separation with color–color diagrams, a photometric redshift ( $z_{\text{ph}}$ ) technique is applied to the galaxy sample for further membership determination. The color–magnitude relation is taken as a further restriction of the early-type cluster galaxies. As a result, 198 galaxies with  $0.081 < z_{\text{ph}} < 0.113$  are selected as faint galaxy members of A98. Based on the enlarged member galaxies and the spatial distribution, localized velocity structures of A98 are discussed. The  $\kappa$ -test algorithm supports the existing substructures A98N and A98S, and the earlier suggested substructure, A98N, becomes more significant.

Assuming a Salpeter IMF and zero initial metallicity, a template SED library with different SFRs and redshifts has been built with the help of an evolutionary synthesis model, PEGASE. We fit the observed SED of 74 member galaxies with known spectroscopic redshifts one by one. The environmental effect on star formation history is found for these member galaxies. The bright massive galaxies in the core region of A98 are found to have shorter SFR time scales, longer mean

stellar ages, and higher ISM metallicities, while the outlier galaxies are likely to have smaller stellar ages and longer SFR time scales. This effect is consistent with the existing correlations, such as the morphology–density relation, the luminosity–metallicity relation, and the mass–metallicity relation.

**Acknowledgements** We acknowledge the anonymous referee for his/her thorough reading of this paper and invaluable suggestions. This work was funded by the National Natural Science Foundation of China (NSFC) (Grant Nos. 10778618 and 10633020), and by the National Basic Research Program of China (973 Program) (Grant No. 2007CB815403). This research has made use of the NED, which is operated by the Jet Propulsion Laboratory, California Institute of Technology, under contract with the National Aeronautics and Space Administration. We would like to thank Prof. Kong, X. at the University of Science and Technology of China for the valuable discussion.

## References

- Abell, G. O. 1958, *ApJS*, 3, 211  
 Abell, G. O., Corwin, H. G., Jr., & Olowin, R. P. 1989, *ApJS*, 70, 1  
 Allen, D. A. 1976, *MNRAS*, 174, 29  
 Beers, T. C., Flynn, K., & Gebhardt, K. 1990, *AJ*, 100, 32  
 Beers, T. C., Geller, M. J., & Huchra, J. P. 1982, *ApJ*, 257, 23 (BGH)  
 Beers, T. C., Gebhardt, K., Forman, W., Huchra, J. P., & Jones, C. 1991, *AJ*, 102, 1581  
 Bettoni, D., Moles, M., Kjærgaard, P., Fasano, G., & Varela, J. 2006, *A&A*, 452, 811  
 Bolzonella, M., Miralles, J.-M., & Pelló, R. 2000, *A&A*, 363, 476  
 Bower, R. G., Lucey, J. R., & Ellis, R. S. 1992, *MNRAS*, 254, 589  
 Brunner, R. J., & Lubin, L. M. 2000, *AJ*, 120, 2851  
 Burns, J. O., Rhee, G., Owen, F. N., & Pinkney, J. 1994, *ApJ*, 423, 94  
 Colberg, J. M., White, S. D. M., et al. 2000, *MNRAS*, 319, 209  
 Colless, M., & Dunn, A. M. 1996, *ApJ*, 458, 435  
 Dressler, R. 1978a, *ApJ*, 223, 765  
 Dressler, R. 1978b, *ApJ*, 226, 55  
 Dressler, R. 1980, *ApJ*, 236, 351  
 Duus, A., & Newell, B. 1977, *ApJS*, 35, 209  
 Faber, S. M., & Dressler, A. 1977, *AJ*, 82, 187  
 Fan, X., Burstein, D., Chen, J.-S., et al. 1996, *AJ*, 112, 628  
 Finoguenov, A., Guzzo, L., Hasinger, G., et al. 2007, *ApJS*, 172, 182  
 Fioc, M., & Rocca-Volmerange, B. 1997, *A&A*, 326, 950  
 Fioc, M., & Rocca-Volmerange, B. 1999, *A&A*, 351, 869  
 Forman, W., Bechtold, J., Blair, W., Giacconi, R., van Speybroeck, L., & Jones, C. 1981, *ApJ*, 243, L133  
 Forman, W., & Jones, C. 1982, *ARA&A*, 20, 547  
 Garnett, D. R., & Shields, G. A. 1987, *ApJ*, 317, 82  
 Geller, M. J., & Peebles, P. J. E. 1973, *ApJ*, 184, 329  
 Gunn, J. E., & Stryker, L. L. 1983, *ApJS*, 52, 121  
 Henry, J. P., & Briel, U. G. 1993, *Adv. Space Res.* 13, (12)191  
 Henry, J. P., Henriksen, M. J., Charles, P. A., & Thorstensen, M. J. 1981, *ApJ*, 243, L137  
 Ilbert, O., Capak, P., Salvato, M., et al. 2009, *ApJ*, 690, 1236  
 Jones, C., & Forman, W. 1999, *ApJ*, 511, 65  
 Kauffmann, G., Colberg, J. M., Diaferio, A., & White, S. D. M. 1999, *MNRAS*, 307, 529  
 Krempeć-Krygier, J., & Krygier, B. 1995, *A&A*, 296, 359 (KK95)  
 Lequeux, J., Rayo, J. F., Serrano, A., Peimbert, M., & Torres-Peimbert, S. 1979, *A&A*, 80, 155  
 Melbourne, J., & Salzer, J. J. 2002, *AJ*, 123, 2302  
 Oegerle, W. R., & Hill, J. M. 1994, *AJ*, 107, 857

- Pelló, R., Kneib, J. P., Le Borgne, J. F., et al. 1999a, *A&A*, 346, 359
- Pelló, R., Kneib, J. P., Bolzonella, M., & Miralles, J. M. 1999b, in *ASP Conf. Ser.*, 191, 241
- Pinkney, J., Burns, J. O., Ledlow, M. J., et al. 2000, *AJ*, 120, 2269 (PBLGH)
- Poggianti, B. 2004, *Proceedings of Baryons in Dark Matter Halos*, Novigrad, Croatia, 5-9 Oct 2004, eds. R. Dettmar, U. Klein, & P. Salucci (SISSA, *Proceedings of Science*), 104.1
- Rhee, G. F. R. N., van Haarlem, M. P., & Katgert, P. 1991, *A&A*, 246, 301
- Rowan-Robinson, M., et al. 2008, *MNRAS*, 386, 697
- Salpeter, E. E. 1955, *ApJ*, 121, 161
- Salvador-Solé, E., González-Casado, G., & Solanes, J. M. 1993, *ApJ*, 410, 1
- Sarazin, C. L. 1992, in *Cluster and Superclusters of Galaxies*, ed. A. C. Fabian (Dordrecht: Kluwer), 131
- Struble, M. F., & Rood, H. J. 1999, *ApJS*, 125, 35
- Tremonti, C. A., et al. 2004, *ApJ*, 613, 898
- West, M. J., Villumsen, J. V., & Dekel, A. 1991, *ApJ*, 369, 287
- West, M. J., Jones, C., & Forman, W. 1995, *ApJ*, 451, L5
- Xia, L.-F., Zhou, X., Ma, J., et al. 2002, *PASP*, 114, 1349
- Yang, Y.-B., Zhou, X., Yuan, Q.-R., Jiang, Z.-J., Ma, J., Wu, H., & Chen, J.-S. 2004, *ApJ*, 600, 141
- Yuan, Q.-R., Zhou, X., Chen, J.-S., Jiang, Z.-J., Ma, J., Wu, H., Xue, S.-J., & Zhu, J. 2001, *AJ*, 122, 1718
- Yuan, Q.-R., Zhou, X., & Jiang, Z.-J. 2003, *ApJS*, 149, 53
- Yuan, Q.-R., Zhao, L.-F., Yang, Y. B., et al. 2005, *AJ*, 130, 2559
- Zabludoff, A. I., Huchra, J. P., & Geller, M. J. 1990, *ApJS*, 74, 1
- Zeldovich, I. B., Einasto, J., & Shandarin, S. F. 1982, *Nature*, 300, 407
- Zhou, X., Chen, J.-S., Xu, W., et al. 1999, *PASP*, 111, 909
- Zhou, X., Jiang, Z.-J., Ma, J., Xue, S.-J., et al. 2003a, *A&A*, 397, 361
- Zhou, X., Arimoto, N., Tanaka, I., Jiang, Z.-J., & Chen, J.-S. 2003b, *PASJ*, 55, 891